An investigation on the development of toppling phenomena at the edge of fractured rock plateaux using a numerical modelling approach

Margherita Cecilia Spreafico[a], Federico Cervi[a], Mirko Francioni[b], Doug Stead[c], Lisa Borgatti[a]

a. Department of Civil, Chemical, Environmental and Materials Engineering DICAM, Alma Mater Studiorum Università di Bologna, Italy
b. Camborne School of Mines, University of Exeter, Cornwall, United Kingdom
c. Engineering Geology and Geotechnics Research Group, Department of Earth Sciences, Simon Fraser University, Vancouver, BC, Canada

ABSTRACT

The mechanisms controlling the onset of minor slope instability at the edges of rocky plateaux exhibiting lateral spreading phenomena are yet to be fully understood. Hypotheses have recently been introduced to explain the influence of groundwater within these plateaux on geomorphological processes leading to slope instability. We present a back analysis of a recent landslide which occurred on 27th February 2014 in the town of San Leo, Italy. The role of the softening of basal clay shales and erosion due to seepage is investigated using finite element geomechanical models. Both processes were observed in the field and are related to groundwater discharging along the contact between the rocky slab and the clay-rich substratum. Fracture propagation paths involving pre-existing discontinuities and intact rock bridges failure were simulated using a simplified Discrete Fracture Network (DFN) model coupled with a Voronoi polygonal mesh approach. Model results allow the failure to be classified as a secondary toppling phenomenon. Moreover, a critical amount of undermining was indicated by the models agreeing with field observations made prior to the failure. Based on the modelling results, an interpretation of the overall mechanism inducing failures at the edges of fractured rock slabs is given. In particular, the inter-relationships between groundwater flow and geomorphic processes acting within the rock masses are presented.

KEYWORDS: SECONDARY TOPPLING, LATERAL SPREADING, UNDERMINING, FEM, VORONOI, NORTHERN APENNINES

Introduction

Deep-seated gravitational slope deformations (DGSDs) may involve large parts of a rock slope and are often classified as sackungen and lateral spreads, depending on the observed slope deformation mechanisms (Dramis, 1985; Soldati, 2013). In both cases, the overall movements are generally slow and the principal hazards encountered are often due to secondary instability phenomena developing within the DSGSD slope (Agliardi et al., 2001; Bonnard et al., 2004). Where lateral rock spreading phenomena involve brittle rock units overlying a more ductile substratum, associated secondary instabilities such as rockfall, toppling and rock slides may occur. These instabilities generally affect the edges of the plateau, while earth slides and earth flows can impact the underlying terrains (Pasuto and Soldati, 2013). Such a variety of mechanisms, specifically related to the long-term evolution of DGSD, can lead to a high level of risk for elements located both at the top and at the base of the rock slabs. Several examples have been described in Europe and particularly in the northern Apennines area of Italy, where historical villages were often built on the top of plateaux. Both tourist and historical sites suffer from similar phenomena in the Maltese archipelago (Gigli et al., 2012; Mantovani et al., 2013). The differential movement of the travertine blocks on which it was built is suggested to be the main cause of processes endangering the Spis castle in Slovakia (Benko, 1997; Vlcko, 2004). Slope instability phenomena endangering the towns of Orvieto, Civita di Bagnoregio and Pitigliano (Central Italy) have been recognized and investigated

46 (Cencetti et al., 2005; Delmonaco et al., 2009; Fanti et al., 2012). The marked contrast between the mechanical
47 properties of the overlying and underlying geological units was indicated as one of the main causes for lateral
48 spread. This has been confirmed by Casagli (1994) and D'Ambra et al. (2004) using 2D continuum numerical
49 models that investigated the resulting stress distributions within the slabs. Other influencing factors have been
50 recognised, including for example stress relief in the stiffer overlying units due to the erosion of the underlying
51 softer units (Bozzano et al., 2008) and overburden load due to the rock slabs causing deformation of the
52 underlying weaker terrains (Pasuto and Soldati, 2013).
53 On the 27th of February 2014 a large landslide endangered the historical centre of San Leo, a medieval town
54 built on the top of a calcarenitic slab (Fig. 1). A volume of about 330,000 m^3 of rock detached from the north-
55 eastern side of the plateau, resulting in the evacuation of several private houses, a primary school and a police
56 station (Borgatti et al., 2015). Before the failure, severe undermining of the rock slab was noticed in the area of
57 the failure, as a result of the progressive removal of the clay shale units. As this erosional process was thought to
58 be associated with surface runoff and shallow landslides occurring in the surrounding small-scale catchments,
59 countermeasures such as earthen dams and retaining walls founded on piles were designed to avoid further slope
60 instabilities. Recently, Spreafico et al. (2015a, b) described the aquifer-characteristics of the calcarenitic plateau.
61 The complex network of fractures and joints generates a relatively high secondary permeability with respect to
62 the clay shale substratum; several perennial springs, fed by the groundwater within the slab, are observed at the
63 base of the cliffs. The erosion from emerging spring water is referred to as seepage erosion and/or groundwater
64 sapping (Dunne, 1980). In bedrock headwalls, with a contrasting bi-modal stratigraphy, seepage weathering
65 precedes erosion at the seepage face and, if favourable joint intersections are present, caves can develop (Lamb
66 et al., 2006). This leads to the progressive undermining, collapse and retreat of the headwall, creating
67 amphitheatre-headed valleys (Nash, 1996). Rock mass failures in the cliffs can thus also be related to the
68 weathering and erosion occurring at the contact between the rocky slab and the basal clay-rich units (Spreafico et
69 al., 2015a). During the investigations undertaken after the occurrence of a similar landslide, affecting the
70 northern cliff of San Leo in 2006, a 3 m thick softened layer was recognised (Gibertoni, 2007). This has been
71 confirmed by more recent surveys carried out in the proximity of the 2014 landslide, indicating a softened layer
72 of approximately 6 m thickness (Lucente, personal communication). In a similar geological context, Picarelli et
73 al. (2006) and Di Maio et al. (2013) highlighted the presence of softened layers outcropping in the southern
74 Apennines of Italy: these layers are characterized by high plasticity clay shales, with thickness reaching 10 m.
75 The softening of the clay-rich layer and/or the undermining of the slab at San Leo could have caused the onset of
76 toppling phenomena, as previously described within the literature in similar environments. Goodman and Bray
77 (1976) describe in detail different types of toppling phenomena. Among these, secondary toppling failures are
78 characterized as failures triggered by undercutting due, for example, to the weathering or the removal of the
79 underlying materials. Evans (1981) focused his work on secondary toppling slope processes investigating
80 possible failure mechanisms and describing the weathering pattern in claystones underlying sandstone cliffs.
81 Since both erosion and softening have been detected at San Leo, the recent slope detachment failure is suggested
82 to be due to this form of secondary toppling phenomena. Tommasi (1996) investigated the methods that have
83 been used to study similar slope stability mechanisms and suggested that toppling caused by the weathering of
84 the underlying materials can be correctly interpreted only with the aid of numerical methods (Finite Elements,
85 Finite Difference and Distinct Element Methods). Spreafico et al. (2015c) conducted a back analysis of the San
86 Leo 2014 landslide using the Distinct Element Method (DEM) code 3DEC (Itasca™, 2014a). Their results
87 highlighted the importance of slope undermining as a predisposing and/or triggering factor, although the failure
88 surface was not fully reproduced with the DEM code.
89 We present in this manuscript a back analysis of the San Leo 2014 landslide with the objectives of better
90 understanding the secondary instability phenomena developing at the edges of the plateau and recognition of the
91 mechanisms acting on the slope in the medium- to long-term (i.e., decades to centuries). The Finite Element
92 Method (FEM) code Phase2 (now called RS2, Rocscience Inc., 2014a) was used to simulate the event. This
93 FEM code has been widely used to simulate similar slope failures. Styles et al. (2011) used Phase2 to back
94 analyse the Joss Bay Chalk cliff failure where the progressive development of a wave-cut notch at the base of a
95 coastal cliff was modelled using simulated model excavation stages. Sturzenegger and Stead (2012) used Phase2
96 to model the Palliser Rockslide, Canada, as a stepped failure surface, while Kasmer et al. (2013) assessed the
97 stability of natural slopes prone to toe erosion in Cappadocia (Turkey).

98 Based on field evidence, two main simulations of the San Leo slope were conducted, in order to consider two
99 possible processes leading to failure: (1) the softening of a relatively thin clay shale layer (5 m thick) and (2) the
100 undermining of the rocky slab. To investigate the critical conditions leading to the 2014 San Leo slope failure,
101 different softening/undermining rates were simulated by (1) considering progressively lowered values of the
102 mechanical properties or (2) assuming different extent in term of length of the undermined area. In both the
103 procedures (1 and 2) the role of a main iron-stained pre-existing discontinuity, observed in the cliff after the
104 failure, was investigated.
105 Simulation method (2) was chosen to investigate the influence of groundwater within the rock slab on slope
106 instability. In particular, the role of the assumed groundwater level and the effect of the water pressure acting on
107 the main discontinuity were taken into account. Simulation method (2) was finally used to demonstrate the
108 potential use of a polygonal Voronoi tessellation approach to simulate fracture of discontinuous rock masses
109 using the continuum code, Phase2.
110 Using the Voronoi approach we show the combined importance of intact rock bridge failure and fracture
111 networks on the failure mechanism within the rock slab. The application of the Voronoi approach in rock
112 engineering using Distinct Element Method codes has been recently described by several authors. Gao and Stead
113 (2014) applied this approach to brittle fracture modelling at laboratory and field scale; Havaej et al. (2014)
114 successfully simulated biplanar failure mechanisms in footwall slopes, while Vivas Becerra (2014) carried out a
115 fully coupled hydro-mechanical analysis on open pit rock slopes using the Voronoi method implemented in the
116 2D UDEC code (Itasca^{TM}, 2014b). The DEM Voronoi procedure for intact rock fracture simulation provides
117 further insights into the failure propagation within a rock mass. In our work we show clearly that the Voronoi
118 approach can also be used within continuum codes such as Phase2 to simulate intact rock failure within rock
119 slopes.
120 Detailed slope investigations are still lacking in the field of lateral spreads and related landslides (Pasuto and
121 Soldati 2013) and more research is required on the stability of slopes in weak rock masses (Picarelli, 2015;
122 Stead, 2016). In this context, our work attempts to unravel the mechanisms driving the development of
123 secondary toppling phenomena at the edges of rocky plateaux. We use numerical modelling to explore and
124 reproduce particular geomorphological processes acting on the slope, which are then related to the behaviour of
125 aquifers within the rocky slabs.

126 **Case study: the San Leo lateral spread**

127 Several Epiligurian slabs stand out on the gentle clayey slopes of the Marecchia valley. Historical towns were
128 built on the top of almost all of them, mostly due to their favourable strategic positions. Among them, the San
129 Leo plateau (43°53'47.87"N, 12°20'35.61"E, about 590 m a.s.l.,) is a well-known cultural heritage site. The
130 boundaries of the slab were over the centuries shaped by several slope instability phenomena (Benedetti et al.,
131 2013).

132   **2.1   Geological and geomorphological settings**

133 The study area is part of the northern Apennines, a fold and thrust foreland belt. Two geological units outcrop in
134 the study area: the Ligurian scaly clays and the Epiligurian limestones and sandstones, forming the so-called Val
135 Marecchia Nappe. The scaly clays were deposited between the Cretaceous and middle Eocene in a deep marine
136 environment and then translated up to their current position overthrusting the autochthonous Umbro-Marchean-
137 Romagnan domains. During the last translational phases, the semi-allochthonous Epiligurian units were
138 deposited in minor sedimentary basins (piggy-back basins), formed within the Ligurian units. The mechanism of
139 the emplacement of the Nappe is still under debate, explained in turn as a gravitational olistostrome (Flores,
140 1955), a gravitational slide (Merla 1951; De Feyter, 1991) or compression in an active roof duplex (Bettelli et
141 al., 1987; Conti, 1989). The landscape of the Val Marecchia Nappe area is characterised by isolated rocky buttes,
142 plateaux and spurs of different dimensions, emerging from gentle hillslopes and badlands. The landforms are
143 controlled by the litho-structural features of the Nappe and by differential erosion processes. The outcropping of
144 resistant rocks and clay-rich terrains promotes selective erosion, shaping steep cliffs and spurs. The clayey
145 substratum is involved in accelerated erosion processes leading to the progressive undermining of rock slabs and
146 cliff retreat together with extensive mass movements and badlands (Nesci et al., 2005; Giardino et al., 2015).
147 The emplacement of the nappe led to the strong deformation of the Ligurian deposits (Vannucchi et al., 2003)

148 which has resulted in highly fissured and overconsolidated fine materials. The heterogeneity and the complexity
149 of the tectonic history makes the assessment of the mechanical behaviour of this unit quite difficult (Casagli,
150 1994). In addition, due to the overthrusting mechanism, the original thickness is not known with confidence. As
151 highlighted by several authors (Casagli, 1994; Froldi et al., 1994), the material becomes stiffer with increasing
152 depth.
153 In the San Leo slab (Fig. 1), a 500 m long and 600 m wide plateau, two units belonging to the Epiligurian
154 domain can be recognised: the San Marino limestones and the Monte Fumaiolo sandstones, lying unconformably
155 on the Argille Varicolori scaly clays. The whole slab has a general north-westward dip and is bordered by
156 approximately 100 m high, sub-vertical and overhanging cliffs. The rock mass is highly fractured. In particular,
157 the northern, eastern and southern sides of the slab show a higher degree of fracturing, while the western side is
158 more massive (Spreafico et al., 2015d).

160 ## 2.2 Climatic and hydrogeological settings

161 In the study area, the mean annual rainfall varies from 369 mm to 1,258 mm (2002-2011; the San Marino rain
162 gauge, located 9 km west of San Leo). During the year, two main rainfall peaks are recognizable, the first
163 between October and November and the second in April. The snow cover is variable; it is usually recorded,
164 according to the ARPA dataset (http://www.arpa.emr.it/sim/?telerilevamento/innevamento), between December
165 and March. In recent years the cumulative snow cover has varied from 7 (2009) to 307 (2012) cm. The mean
166 annual temperatures range between 11.7° C and 14.5° C, with a maximum of 27.6° C in July and August and a
167 minimum of 0.4° C in January. The mean annual effective rainfall was estimated as 223 mm using the
168 Thornthwaite and Mather (1957) formula and can be supplied to the soil between October and May. As noted by
169 Spreafico et al. (2015b), this aliquot of water supplies a unique aquifer hosted within the calcarenitic slab, which
170 in turn feeds several perennial and ephemeral springs discharging near the contact with the underlying clayey
171 substratum. Springs discharges follow closely the effective rainfall distribution, with maximum values of a few
172 ls^{-1} occurring from February to April. In this period, the time-lag between rainfall and discharge rise can be in the
173 range of a few hours (Spreafico et al., 2015b).

175
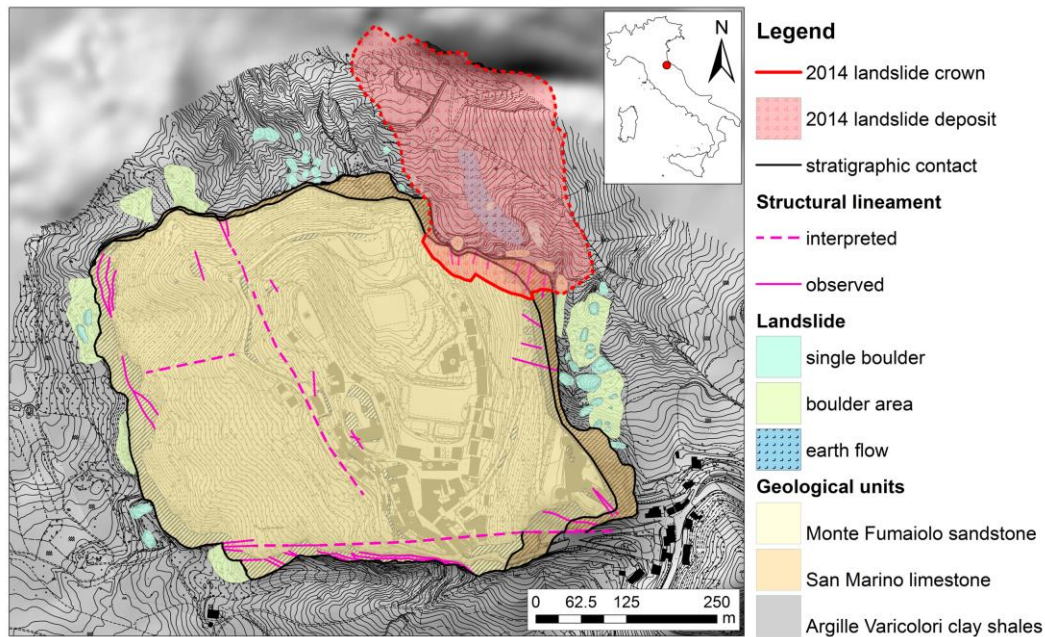
176 ***Fig. 1*** *Pre-event geological and structural map of the San Leo rock slab, the red line shows the area involved in the 2014*
177 *landslide (modified after Badioli, 2012).*

178 ## 2.3 Typical slope instability phenomena and evolution of the San Leo plateau

179   The study area has for centuries been affected by slope instability phenomena. Benedetti et al. (2013) examined
180   several ancient documents and highlighted the similarity of the oldest recorded landslides with those recently
181   occurring. As mentioned previously, the overall mechanism can be described as a lateral spread, or rock spread
182   following the definition of Pasuto and Soldati (2013). Cruden and Varnes (1996) described block spreads as
183   movements which involve a thick layer of rock overlying softer materials. Hungr et al. (2014), in a recent update
184   of the Varnes classification, used the term rock slope spreading to indicate the quasi-horizontal stretching of a
185   mass of coherent blocks of rock (cap rock), resulting from the deformation of the underlying weak material or by
186   multiple retrogressive sliding. In addition to the contrast between the two overlapping units (rocky slab and clay-
187   rich substratum), the phenomena are probably driven by the relatively slow processes developing in the clay
188   shale unit, which in turn trigger more rapid mass movements at the edges of the rock slab. The low material
189   mechanical properties, the infiltration of water and other external factors can trigger shallow movements in the
190   clayey slope, causing removal of material at the contact between the slab and the substratum. The role of the
191   water discharging from the aquifer hosted within the slab appears to be very important, promoting the
192   erosion/softening of the clayey material and the subsequent undermining of the rock faces. The resulting stress
193   regime induces the progressive opening of the fractures in the rock mass, which in turn leads to higher discharge
194   rates in the springs and enhanced erosion. The resulting rockfalls, toppling and slides may cause undrained
195   loading of the saturated clayey slopes resulting in the reactivation or the acceleration of the landslide bodies at
196   the foot of the cliffs. In addition, depending on the orientation of the fractures relative to the water gradient,
197   groundwater flow within the rock mass can influence the stress conditions in the rock slab. The water pressure
198   acting within a discontinuity can reduce the effective normal stresses and hence decrease the shear strength or
199   cause additional seepage/tension crack forces.
200   On the 11th May 2006 about 50'000 m^3 of rocks detached from the northern side of the slab, causing the
201   reactivation of an ancient earth flow at the base of the cliff. Laboratory and in-situ tests were performed on the
202   clayey terrains. In particular an upper layer (1-3 m thick) with reduced mechanical properties, with respect to the
203   deeper layers, was recognized. Moreover, during field surveys conducted in 2014 in the same areas, several rock
204   detachments were observed, especially at the base of the cliffs (Spreafico et al., 2015d). In these areas no
205   erosional features have yet developed. The phenomena mostly comprised wedge failures involving at least two
206   pre-existing joint-sets (Fig. 2a). They are always associated with the presence of the softened clay shale layer,
207   along which the wedges can slide (Fig. 2a). The pre-existing joint sets act as lateral release surfaces for the
208   wedge and a fully-formed sliding surface can be recognized in the clay shales. Probably, the induced stress
209   causes the developing of a rear newly-formed surface, resulting from pre-existing joints and intact rock bridge
210   fracture.
211   On 27th February 2014 a failure occurred in the north-eastern cliff involving a volume of about 330'000 m^3 of
212   rock. After the event, a major pre-existing discontinuity plane, about 65 m long and 40 m wide, was recognized
213   in the upper part of the landslide scarp (discontinuity SL3.1 in Fig. 2b and c). From observations of the
214   weathering of the surface, it is suggested that this discontinuity was probably already open before the failure.
215   Several field surveys conducted after the landslide allowed discontinuities with similar orientation to be
216   identified in the area bordering the north-eastern cliff and showed a mean spacing of about 20-22 m (Enser srl,
217   2014). In the lower area of the landslide scarp, the failure seemed to propagate along smaller minor joints and
218   through the fracture of intact rock bridges, showing a backward-propagation (Fig. 2d, red line). Terrestrial Laser
219   Scanner (TLS) surveys were performed pre- and post-failure and allowed the identification of the main
220   discontinuity sets in the area affected by the 2014 landslide (Spreafico et al., 2015c). Sections from the TLS
221   point clouds are presented in Fig. 2d and 4a. The surveys conducted before the failure highlighted the presence
222   of undermining in the area: caverns extending about 20 m under the slab were indicated (Fig. 4b). The precise
223   quantification of the extent of undermining was however not possible, due to the rough topography and to
224   rockfall hazard at the base of the cliff.
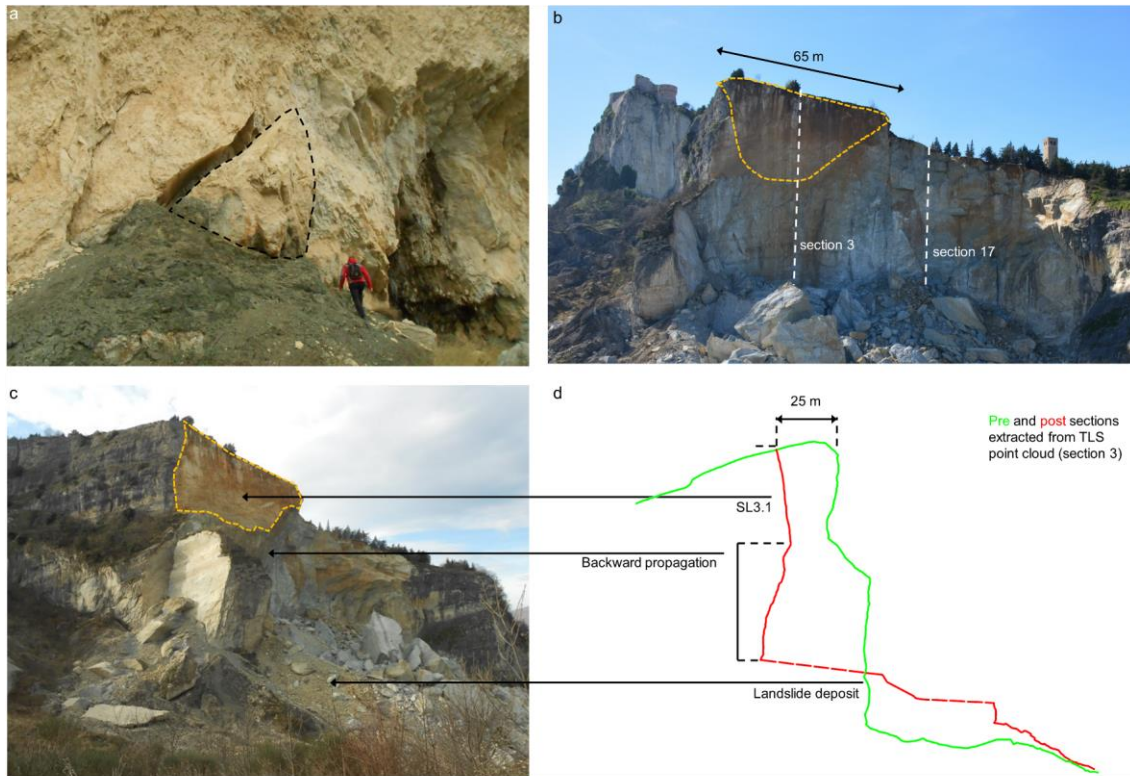
Fig. 2. *Views and sections of the San Leo plateau a) rock wedge detachment observed in the area of the 2006 landslide; b and c) views of the landslide area: the dashed yellow line borders the discontinuity referred to as SL3.1; d) section 3 from TLS, shown in green is the pre-failure surface and in red the post-failure surface. For section 17 see Fig. 4. Section numbers are reported in Spreafico et al. (2015c).*

2.4   Chemical alteration and physical weathering in the basal clay-rich units

Spreafico et al. (2015c) highlighted that the slope instability phenomena developing in the San Leo area are predominantly driven by the behaviour of the basal clay shales. As mentioned, the latter are composed of clay-rich units that are the result of a complex geological history, whose effects on their mechanical behaviour are noted by Picarelli et al. (2000). Due to aforementioned tectonic stresses, the clay shales appear sheared and highly fissured. Fissure/fracture surfaces are often polished and slickensided, with the development of fragments whose size varies from millimeters to centimeters (fig. 3a). As suggested by Picarelli et al. (2006), the peak strength can be close to residual, along closely-spaced discontinuities. The same authors noted that other mechanisms such as weathering, cycles of wetting-drying or freezing-thawing can promote a reduction in the shear strength values (i.e., the softening). Softening as described by Terzaghi (1936), Skempton (1970) and Nakano (1979), i.e. due to water absorption upon unloading, has been classified as an internal process, while softening due to weathering, has been considered to be external (Yoshida, 1991). Almost all of these mechanisms act on the superficial soil layers (up to 10 m), and are driven by water percolation, facilitated by the presence of shrinkage-induced cracks in the soil taking place during the dry season (fig 3b) and stress release (Picarelli et al., 2005; Yoshida, 1990). Water infiltration plays a fundamental role in the softening of clay rich terrains (Miscevic and Vlastelica, 2014) inducing chemical alteration (dissolution and precipitation of minerals; variation in pore water chemistry) and physical weathering (erosion s.s.). In particular, the first phenomenon can be described as the decomposition of the existing minerals to stable or metastable secondary mineral products, while the latter is related to the mechanical disaggregation of the former rock (Miscevic and Vlastelica, 2014). Both chemical and physical processes have been identified in similar highly plastic clay shales outcropping in the Italian Apennines (Picarelli et al., 2006; Picarelli and Di Maio, 2010). Here, two different mechanisms of soil weakening have been recognized: a) the reduction of effective shear strength parameters due to exposure to fresh water, associated with the progressive change of the chemical composition of the pore fluid, and b) a decrease in the soil suction pressure within unsaturated soils, which leads to a reduction of the associated apparent cohesion.

Fig. 3. *Photographs of the clay shales outcropping in the San Leo area: a), c) and d) at the contact with the rock slab at the base of the northern cliff; b) example of shrinkage-induced cracks in the proximity of the 2006 landslide deposit.*

With reference to (a), pore water chemistry is a well-known factor influencing the shear strength of clayey materials (Kenney, 1967; Mesri and Olson, 1970; Di Maio, 1996a, b; Di Maio et al., 2014). In particular, soils composed of clay minerals such as Smectite (i.e., sodium montmorillonite) are the materials most influenced by this process, due to the mutual role of Na and Ca cations with respect to this phase and the consequent changes in the interparticle forces. This is the case in the highly fissured plastic clay shales, which were initially deposited in a marine environment (Na-rich water) and only afterward exposed to rainfall and snowmelt infiltration (Ca-rich water). This leads to the replacement of Na with Ca within the pore water, inducing a change in clay-structure and a consequent reduction in shear strength (Picarelli et al., 2003; Di Maio and Onorati, 2002). The same process may reflect a decrease in the cohesion (Picarelli et al., 2006), peak and residual friction angles (Di Maio, 1996b; Di Maio et al., 2004). In addition, replacement of Na with Ca can enhance volumetric strains induced by swelling already acting on the clayey materials (Calabresi and Scarpelli, 1985; Rampello, 1992) leading to volume increase (Seedsman, 1986; Di Maio et al., 2004). A decrease in the soil suction pressure within unsaturated soils (b), has been shown to influence the mechanical properties of soils (Lu and Godt, 2008; Bittelli et al., 2012). Soils near the ground surface are seldom saturated (Freeze and Cherry, 1979), exhibiting three phases: solid, water and air (Fredlund and Rahardjo, 1993). The development of negative pore water pressures, or suction, influences the effective stress regime (Al-Badran, 2011).

Fredlund and Morgenstern (1978) described the shear strength of unsaturated soils, using the variables $(\sigma - u_a)$ and $(u_a - u_w)$, as:

$$\tau = c' + (\sigma_n - u_a) \tan\phi' + (u_a - u_w) \beta\tan\phi'$$

where τ is the shear strength, c' and ϕ' are the effective cohesion and angle of internal friction, σ_n is the total normal stress on the failure plane, u_w is the pore-water pressure and u_a is the pore-air pressure. The coefficient β represents the ratio between the rate of increase in shear strength relative to a change in matric suction (ϕ^b) and

280   φ'. β varies from 1 (saturated soil, $φ^b = φ'$) to low values (low water contents, $φ^b < φ'$) and accounts for the
281   decrease in the effective stress strength relative to matric suction increase.

282   In the case of unsaturated soils, soil suction plays an important role in defining material properties, e.g. rainfall
283   can cause a decrease in suction and thus in the associated apparent cohesion (Picarelli et al. 2006).

284   These authors, together with Di Maio et al. (2013) reported the presence of a superficial softened layer on the
285   order of some meters thickness within the high plasticity clay shales.

286   Both the mechanisms (a) and (b) were detected in clay shales from the San Leo area. Field and laboratory tests
287   by Gibertoni (2007) have confirmed the presence of an upper softened layer with lower values of cohesion and
288   friction angles, with respect to the lower portion of the substratum. In addition the composition of the soil
289   showed a significant amount of smectite (Ribacchi and Tommasi, 1988) suggesting a high degree of activity and
290   a swelling behaviour. The widespread presence of Thenardite (Na_2SO_4) and Kieserite ($MgSO_4 \cdot H_2O$) is clearly
291   evident in the field (Fig. 3c and d) suggesting the influence of pore-water chemistry.

292   As anticipated, water represents the main driver of these mechanisms; in the San Leo area, water supply is from
293   direct rainfall and from the ephemeral and perennial springs discharging at the contact between the plateau and
294   the clayey units. The water discharging from these springs also induces the seepage erosion of the clayey soils,
295   promoting the undermining at the foot of the cliffs (fig. 4b). Undermining is more pronounced at the locations of
296   the main discharge points (i.e. perennial springs) of the groundwater hosted within the slab.

297   **Materials and methods**

298   The principal objective of the San Leo 2014 failure back-analysis was the investigation of the failure
299   mechanisms acting at the borders of rock slabs affected by lateral spread phenomena. Two main potential
300   predisposing causes of the instability were considered: 1) the softening of a clay shale layer of 5 m thickness,
301   and 2) the undermining of the cliff due to the clay shales erosion enhanced by seepage. Simulations were
302   conducted for both cases using the 2D FEM code Phase2. This software allowed the role played by the major
303   pre-existing discontinuity and by groundwater hosted within the rock slab to be examined. It should be noted that
304   some of the indirect effects of the groundwater level on the substratum, i.e. the chemical and physical
305   weathering, were indirectly taken into account in the numerical simulations by considering (1) degradation of
306   clay shale mechanical parameters or (2) clay shale removal.

307   **3.1   Model geometry and parameters**

308   A Mohr-Coulomb elasto-plastic failure criterion was assumed for all the materials. In all simulations, with the
309   exception of those using the Voronoi tessellation, the discontinuous rock mass was treated as a continuous
310   equivalent medium (Table 1). Considering the objective of the analysis and the similarity of the two units
311   forming the rock slab, the Monte Fumaiolo sandstone and the San Marino limestone were assumed to have the
312   same mechanical properties. Rock mass properties were calculated using the RocLab code (Rocscience Inc.,
313   2014b). An intact uniaxial compressive strength of 99 MPa was assumed based on field-testing results using a
314   Schmidt hammer (Di Giusto, 2009). A Geological Strength Index (GSI; Hoek, 1994; Hoek and Brown, 1997)
315   equal to 50 was initially assumed based on field geomechanical surveys. A value of 1.25 MPa was selected for
316   the tensile strength of the rock mass. The latter falls between the minimum value resulting from the RocLab
317   analysis (0.13 MPa) and the maximum value (6 MPa) based on the back analysis of the cohesion and friction
318   angle values. Moreover, laboratory tests performed on borehole core showed values of the tensile strength of the
319   intact rock ranging between 2 and 4.9 MPa.

320   A Mohr-Coulomb constitutive criterion was assigned to the pre-existing discontinuities (Table 2). Cohesion and
321   friction angle were derived from geomechanical survey. Applying the formulae reported in Barton and Choubey
322   (1977), the normal and shear stiffness were derived from the measured JRC and JCS parameters (Spreafico et al.,
323   2015c).

324   In the Voronoi-DFN model, due to the explicit insertion of the main discontinuities, the GSI of the rock mass
325   was increased to 70. This was done to allow a more realistic downgrading of rock mass parameters (Table 1). In
326   fact, the use of the GSI allows the estimation of the equivalent rock mass properties, taking into account both the
327   intact rock and the discontinuities. In particular, a sensitivity analysis was performed using different values of
328   GSI, attempting to balance both the number of inserted model discontinuities with that observed in the field
329   (with a representative ratio of about one model discontinuity to ten field discontinuities) and discontinuity

importance, i.e. only the discontinuities actively involved in the failure were inserted. In order to allow fracture through the Voronoi contacts alone, elastic properties were assigned to the material included within the Voronoi boundaries. The Voronoi rock mass contacts were characterized with the same cohesion, tensile strength and friction angle as the rock mass (Table 2). The sides of the Voronoi polygons are intended to allow a simulation of the possible intact rock fractures within the intact rock mass. The normal stiffness (k_n) was calculated using the formula proposed by Alzo'ubi (2009). The shear stiffness (k_s) was then estimated using the k_n to k_s ratio reported in Christianson et al. (2006). In this way, the overall Elastic and Shear modulus values of the rock mass were maintained.

Clay shale parameters, reported in Table 1, were derived from literature (Casagli, 1994; Froldi et al, 1994; Ribacchi and Tommasi, 1988; Gibertoni, 2007). A progressive increase in these parameters with depth was assumed in order to account for the data reported in Casagli (1994) and Froldi et al. (1994), which showed that the material becomes stiffer with depth.

Table. 1 *Material parameters used in the numerical modelling (rock mass properties with a GSI of 65 are referred to the parameters chosen for the model after the back-analysis performed on section 17)*

Material	Unit weight (MN/m³)	Young's Modulus E (MPa)	Poisson's ratio v	Cohesion (MPa)	Cohesion (residual) (MPa)	Friction angle (°)	Friction angle (residual) (°)	Tensile strength (MPa)	Tensile strength (residual) (MPa)
Clay shales	0.021	1,500	0.3	0.040	0.032	28	20	0.048	0.045
Rock mass (GSI 65) (Properties chosen after the back-analysis on section 17)	0.024	17,000	0.25	7.2	5.7	39	34	1.25	0.62
Rock mass (GSI 70) (Voronoi-DFN model)	0.024	20,000	0.25	7.8	-	41	-	1.3	-

Table. 2 *Discontinuities and Voronoi parameters used in the numerical modelling. MTL refers to the joint Mean Trace Length*

Discontinuity ID	Dip [°]	Dip direction [°]	MTL pre landslide [m]	Normal stiffness (MPa/m)	Shear stiffness (MPa/m)	Peak Cohesion (MPa)	Peak Friction Angle (°)	Tensile Strength (MPa)
SL1	79	239	6.9	9,500	950	0.029	34.7	-
SL3	84	023	4.4	9,500	950	0.030	34.7	-
SL4	59	043	7.6	9,500	950	0.031	34.9	-
Voronoi	-	-	-	28,000	11,000	7.8	41	1.3

Pre- and post-failure geometries were obtained from the TLS surveys of the cliff (Spreafico et al. 2015c). The section profiles were extracted from the pre-landslide TLS point clouds and extended by using the DTM of the area, in order to ensure minimal influence of the boundary conditions (Fig. 5). The final extent of the model is approximately 600 m (in the x direction) by 400 m (in the y direction). The models were discretized with a graded 6-noded triangle mesh, with a refined grid in the proximity of the edge of the plateau, i.e. the area affected by the failure. A zero y-displacement boundary condition was applied on the vertical sides of the model, while zero x and y-displacements were set for the bottom boundary. Initial conditions were applied by prescribing a gravity load to the entire model. Due to the uncertainty about the in situ stress conditions, horizontal/vertical stress ratios were set equal to 1. In fact, the geological evolution of the Valmarecchia nappe is still under debate. In particular, in the published literature compressional, extensional and gravitational tectonic processes are all described in the evolution of this area. An evaluation of the influence of this factor in similar cases can be found in Casagli (1994). The unit weight of the rigid blocks was assumed to be 24 kN/m³ for the rock slab and 21 kN/m³ for the clayey substratum (Ribacchi and Tommasi, 1988). Two sections were extracted

362 and analysed: the first has been selected as the most overhanging slope (section 17, Fig. 4a), while the second is
363 representative of the pre-failure geometry (section 3, Fig. 2d). Section 17 was used to back-analyse the rock
364 parameters, assuming that, prior to the failure, the factor of safety should have been larger than 1. A Shear
365 Strength Reduction (SSR), approach was used with gradual reduction of the strength parameters of the materials,
366 until failure was reached. A Strength Reduction Factor (SRF) lower than 1 means that the slope is not stable. The
367 application of this method has been discussed by several authors including Hammah et al., (2005), Diederichs et
368 al., (2007) and Hammah et al., (2007). The resulting parameters (Table 1) were subsequently used to perform the
369 simulations on the most representative section (section 3).
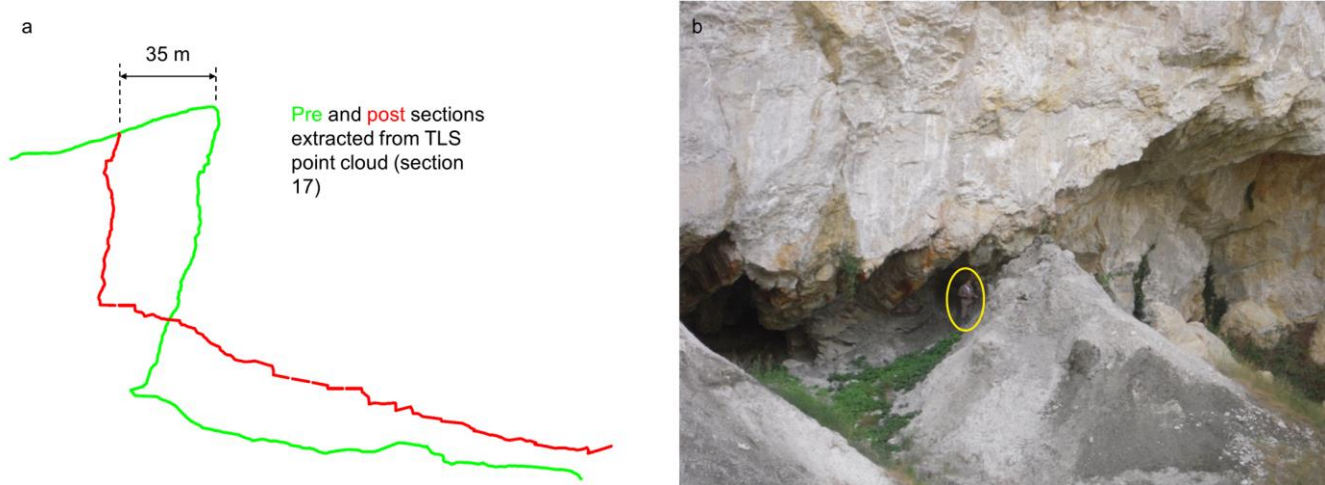
370
371 **Fig. 4. San Leo 2014 event:** *a) section 17 from TLS, shown in green is the pre-failure surface and in red the post-failure*
372 *surface are shown. For the trace section see Fig. 2b; b) pre-failure photographs showing the undermining at the base of the*
373 *cliff and in the yellow circle a person for scale (Photograph courtesy STB Romagna).*

374   **3.2   Model Simulations**

375 The FEM simulations shown in Fig. 5, were performed on the San Leo section 3. For all simulations, the initial
376 steps consisted of the gradual removal of 5 clay shale layers from the top of the model. As suggested by
377 Bozzano et al. (2008), this approach allows simulation of the recent evolution of a slope and the related stress
378 history, i.e. the differential erosion (Fig. 5, step 1 to 5), acting mostly on the softer clay shale unit with respect to
379 the structural surfaces of the rocky slab. An additional simulation was conducted, including the progressive
380 removal of vertical layers from the border of the slab in order to simulate the effects of previous rock
381 falls/topples, similar to the one that occurred in 2014; no significant differences were detected with respect to the
382 first approach for the purpose of the presented analyses.

383
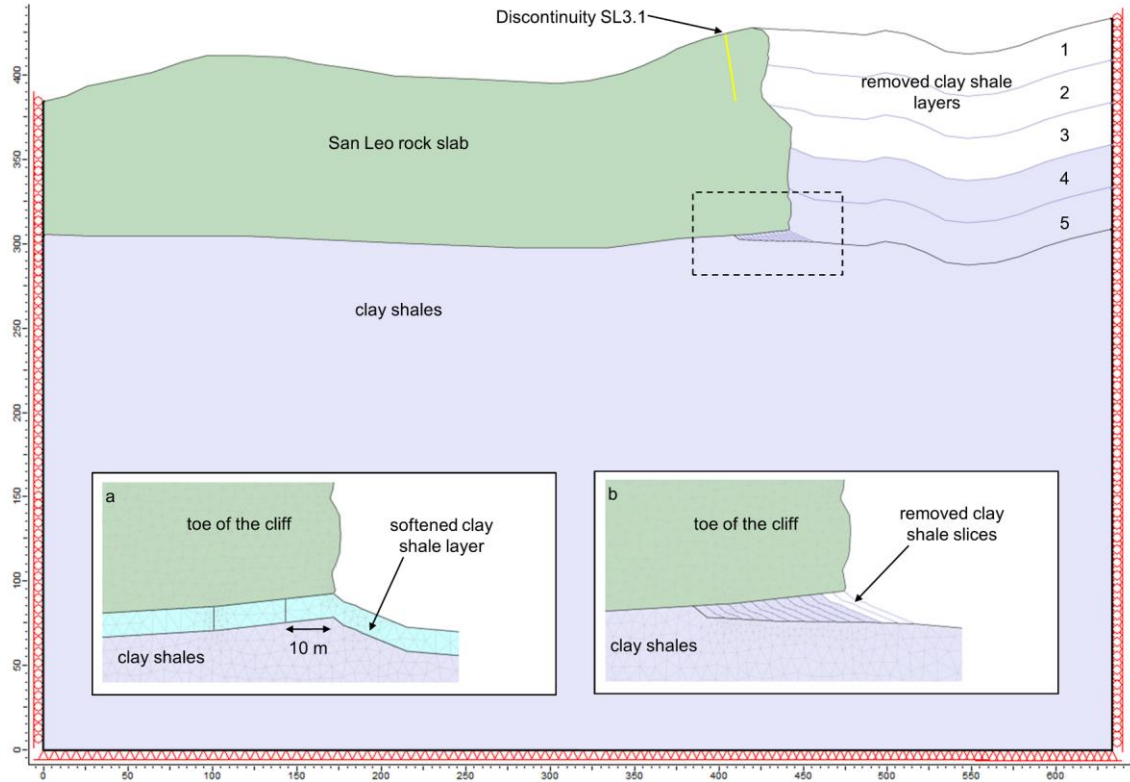
Fig. 5. *Geometry of the Phase2 models and of the two types of simulations undertaken: a) Softening of a thin Clay Shale layer of 5 m thickness (SCSL) and b) Undermining of the slab due to the seepage-related erosion of the clay shales (US). The numbers from 1 to 5 indicate the first stages of the simulations, where the gradual removal of 5 clay shale layers has been undertaken.*

All simulation results were compared with the information collected during geomorphological surveys and TLS data. In particular the TLS post-failure surface was used to validate the numerical results.

A summary of the simulations is illustrated in Fig. 6, where the influence of the insertion of the main discontinuity SL3.1 was studied for the two main potential causes of slope failure: 1) the presence of a Softened Clay Shale Layer (SCSL) and 2) the Undermining of the Slab (US). The influence of variations in the groundwater level and the effect of the water pressure acting on the main discontinuity were taken into account in the US model only. In all previous simulations the jointed rock mass was treated as an equivalent continuous medium, i.e. the discontinuities were inserted implicitly (except for discontinuity SL3.1). The Voronoi approach implemented in the US model incorporated a simplified Discrete Fracture Network, DFN, in order to explicitly simulate the discontinuities, both the pre-existing joints (simulated through the simplified DFN) and the intact rock fractures, represented by the sides of the Voronoi polygons.

Summary of the performed simulations	Softened Clay Shale Layer (SCSL)	Undermining of the Slab (US)
Main discontinuity SL3.1	X	X
Groundwater	-	X
Voronoi approach	-	X
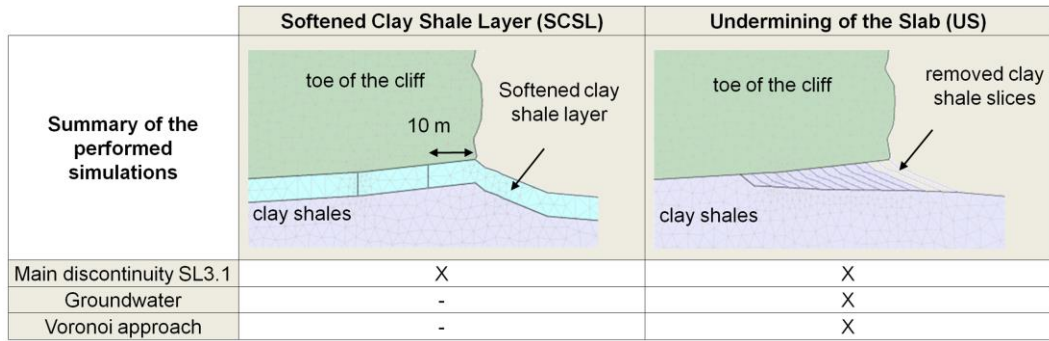
Fig. 6. *Schematic illustration showing the types of simulations performed.*

403 3.2.1 Softened Clay Shale Layer (SCSL)

404 To simulate the clay shale softening, the mechanical properties of a 5 m thick layer were decreased by a factor
405 varying from 0.1 to 0.9. This means that the clay shale parameters, i.e. Young modulus, cohesion, friction angle
406 and tensile strength were decreased from 10 to 90% of their initial values, reported in Tab. 1. The extent of the
407 softened area under the slab is unknown. By analysing claystone weathering pattern in a similar manner to that
408 presented in Evans (1981) and Tommasi (1996) it is suggested that the degree of softening can vary spatially,
409 increasing toward the edges of the plateau. Due to the influence of groundwater flow paths and with reference to
410 the proposed conceptual weathering model, the extent of the softened clayey layer in our FEM models was
411 assumed to vary. In particular, simulations were performed assuming a layer 10, 25 and 50 m in length measured
412 from the toe of the cliff and extending in-slope beneath the plateau. A further simulation was performed with the
413 same layer extending in-slope for the total length of the plateau. A first analysis was conducted to evaluate the
414 failure mechanisms, with and without the insertion of the pre-existing discontinuity SL3.1. The position and the
415 trace length of the discontinuity were deduced from the TLS data. Subsequently, several slope simulations were
416 conducted, varying both the degree of softening and the length of extent of the softened clay layer. The
417 decreased clay shale mechanical properties were then compared with those reported by Gibertoni (2007) and
418 derived from laboratory tests.

419 3.2.2 Undermining of the Slab (US)

420 The modelling scheme consists of several steps in order to simulate the erosional processes driven by
421 groundwater seepage (Fig. 5b). In particular, elongated clay shale slices of 2.5 m were progressively removed
422 starting from the toe of the cliff. The role of the pre-existing discontinuity SL3.1 was analysed through
423 comparative simulations in which it was either omitted or included. An SSR approach was then used, to
424 calculate the SRF for each model step. A SSR Search Area option was adopted which allows focusing of the
425 failure surface search within a particular region of the model, i.e. the area located at the border of the slab; the
426 results allowed the degree of erosion to be correlated with the stability of the slope.

427 3.2.3 Evaluation of the groundwater effects in the US simulation

428 The results of a 3D hydrogeological model (FEFLOW; Diersch, 2005), presented in Spreafico et al. (2015a),
429 were used to show a maximum of 4 m elevation of the groundwater level, prior to the 2014 landslide. To
430 evaluate the influence of the groundwater on the stress conditions and the hydraulic loads acting on the main
431 discontinuity, simulations were performed using the US model (a) including the piezometric line derived by
432 Spreafico et al. (2015a) and (b) considering the hydraulic load on the discontinuity SL3.1.
433 In the US simulation of the groundwater level rise (a):
434   1) the average piezometric line derived from the hydrogeological model was inserted into the US
435   simulation from stage 6, i.e. after the initial stage representing the recent evolution of the slope (i.e.,
436   differential erosion). The insertion of the groundwater surface is expected to make the slope less stable
437   compared to the simulation conducted without water;

438 2) the model was then run until the slope failure was reached, to identify the critical degree of undermining
439   in the simulation with the average piezometric line;
440 3) a new simulation was then undertaken ending the removal of the clay slices at the stage prior to the
441   failure, to test the influence of the groundwater surface rise alone;
442 4) in the following stage the excavation amount remained fixed and the groundwater surface was raised
443   based on the FEFLOW simulation results.
444 For the US simulation concerning the water pressure insertion (b) a similar procedure was adopted:
445 1) the clay shale slices were gradually removed until the stage prior to the failure;
446 2) in the following stage, the removal of a further clay shale slice was substituted with the insertion of the
447   water pressure in the discontinuity SL3.1.
448 This allows estimation of whether an increase in the groundwater level or inclusion of the water pressure in the
449 main discontinuity could be considered as the triggering factor of the failure or not.

450 3.2.4 Implementation of the Voronoi approach in the US simulation

451 As noted by Borgatti et al. (2015), the San Leo slope failure initially developed along a pre-existing
452 discontinuity and then propagated partly through the intact rock mass, with the breaking of intact rock bridges,
453 and partly along other pre-existing discontinuities. The Voronoi tessellation was used to simulate fracture
454 propagation. This tessellation randomly sub-divides the space into non-overlapping convex polygons. The
455 Phase2 code allows the creation of a discrete fracture network allowing simulation of natural joint patterns
456 within the rock mass. The Voronoi joint network consists of joints that are defined by the bounding segments of
457 the Voronoi polygons. The Voronoi logic allows the different blocks formed by the polygons to detach
458 completely from another simulating intact rock fracture and block movement; this approach was implemented in
459 the US model. The density of the joint network was chosen setting the mean length of the Voronoi polygon edge
460 equal to 0.5 m. This allowed simulation of a fine fracture network without an excessive increase in the
461 computational effort. With reference to Gao and Stead (2014), as fractures can only develop along the block
462 contacts, a smaller block size results in a lower influence on the simulated fracture pattern. Due to the major
463 increase in computational runtime due to the insertion of Voronoi polygon and the consequent reduction in the
464 mesh size, the Voronoi were inserted only in the area close to the edge of the plateau, where the failure was
465 expected to develop. In this simulation, the pre-existing discontinuities mapped by means of TLS point cloud
466 were also considered. Three main joint sets were mapped. Results of the discontinuity characterization are
467 described in Spreafico et al. (2015c) and are reported in Table 2. In particular, the average spacing of the joint
468 sets SL1 and SL4 observed in the field during engineering geological surveys was about 0.5 m, while the spacing
469 of joint set SL3 was approximately 2m. In the failure debris area blocks up to 20'000 m^3 are easily recognizable
470 and almost 50% of the failure blocks have a volume larger than 64 m^3. It is therefore suggested that it is clear
471 that not all the discontinuities observed play an active role in the slope failure mechanisms, otherwise the block
472 dimensions would have been significantly smaller. An explanation can be provided by considering the different
473 degree of persistence of the joints and the presence of rock bridges within the rock mass. As an example,
474 observing the slope sketched in Fig. 7, and assuming an average spacing of 0.5 m between the discontinuities
475 slope failure would most probably occur on the more persistent joints, i.e. first order discontinuities, while the
476 others discontinuities may not be actively involved in the failure.
477 To consider only those fractures actively involved in the failure, the spacing was assumed on the basis of the
478 average post-failure block dimensions, assuming that the edges of these blocks can be considered as 1st order
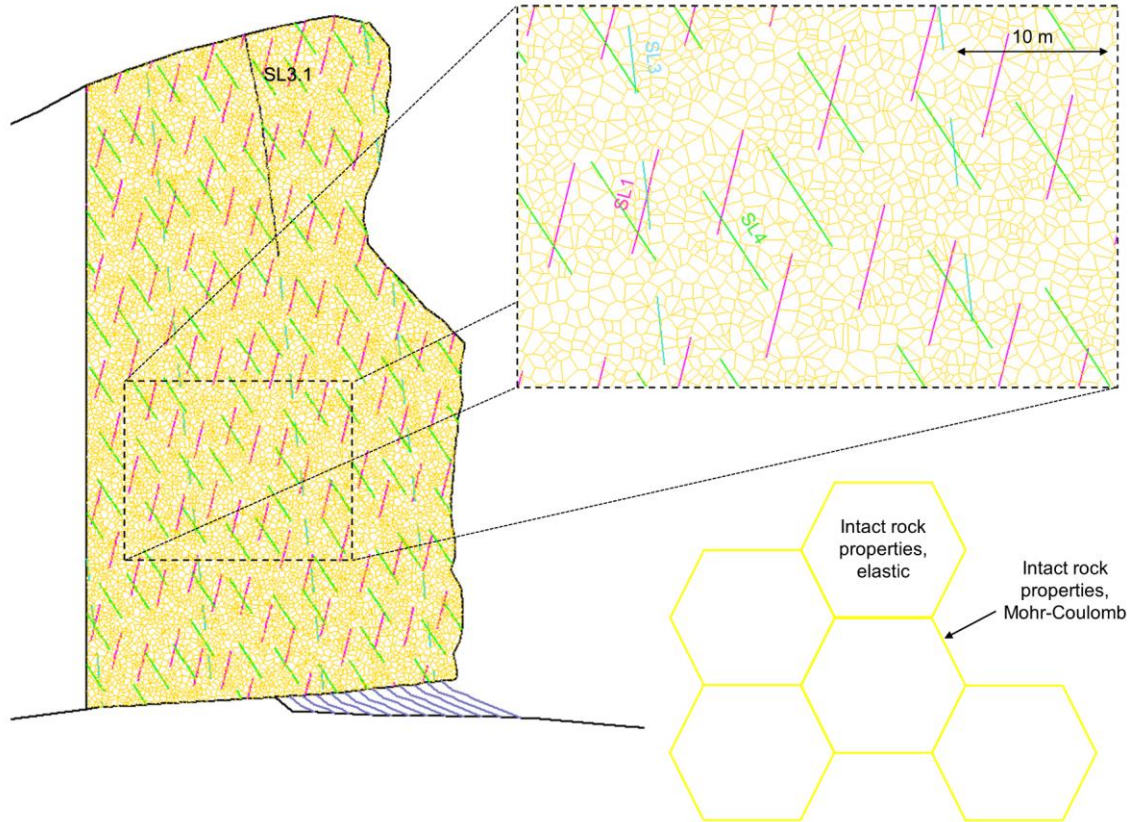479 discontinuities.
480
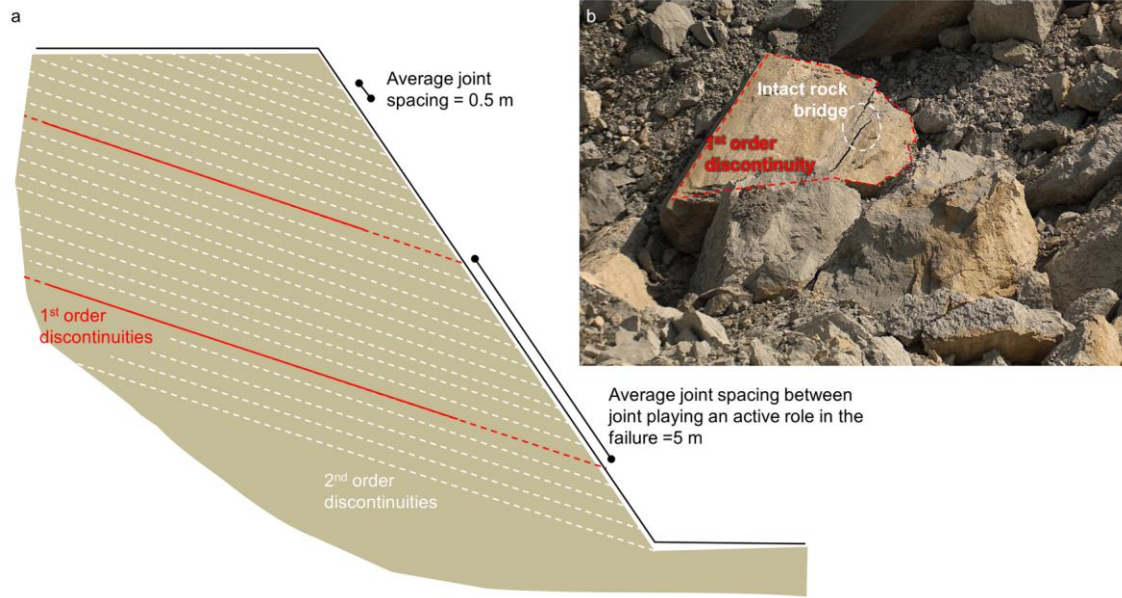
Fig. 7. *Discontinuity characterization: a) sketch of a conceptual slope illustrating the difference between the average joint spacing measured in the field and the effective joint spacing of the discontinuities actively involved in the actual failure mechanism; b) example of 1st order discontinuity and of second order discontinuities, interrupted by intact rock bridges, in the deposit of the 2014 San Leo landslide.*

Three joint networks, each representing one of the joint sets, were introduced into the Phase2 model, using parallel deterministic networks. This simplified Discrete Fracture Network (DFN) was implemented with the aim of evaluating the interaction between the pre-existing discontinuities and their propagation through the intact rock matrix. Using the parallel deterministic network it is possible to choose an infinite joint length, or to specify persistence, defined as the ratio of the joint length to total length along the joint plane. Three scenarios were simulated, varying the persistence of the pre-existing discontinuities between 25, 50 and 75%. Different simulations were performed for each of these scenarios, to account for the probabilistic nature of the DFN generation. The Voronoi contacts were characterized with the same properties of the rock mass, to allow the simulation of the rock mass fracturing. The use of the Voronoi logic allows a more realistic simulation of slope failure and shows fracture initiation and propagation during slope failure (Vivas Becerra, 2014).

Fig. 8. *Geometry of the Voronoi network (in yellow) and of the simple DFN. Shown in magenta, blue and green are discontinuities belonging respectively to the discontinuity sets SL1, SL3 and SL4 (persistence equal to 50%).*

Model Results

In the initial simulation stages step-by-step removal of the clay shale layer promotes an unloading and consequential stress-induced deformation in the clay shales. In all the simulations, squeezing and shear yielding were noticed in the clayey unit at the edge of the plateau.

Both the SCSL and US simulations performed without the insertion of the discontinuity SL3.1 at the top of the slope, showed a failure pattern that did not agree with field observations on the San Leo 2014 failure. In this case, a larger volume of rock mass was involved in the failure and the backward propagation of the failure surface was not reproduced. The insertion of the discontinuity resulted in the simulation of a failure surface that agreed very closely to that measured with the TLS post 2014 San Leo failure; a comparison is shown in Fig. 11.

3.3 Softened Clay Shale Layer (SCSL)

Various degrees of softening and different lengths of in-slope extent of the softened clay shales layer were investigated. Analyzing the maximum shear strain values and the yielded elements (i.e. mesh elements which failed in shear or tension) it is possible to recognize which combination of parameters was critical for the onset of slope instability. In Fig. 9, the most relevant simulation results are shown. In the upper row of fig, 9 the alteration degree was fixed at 80 % of the initial values, while the lateral extent of the softened layer was increased in length. The slope reached a critical state when the softened layer was extended under the entire length of the slab. Simulations carried out using a reduced extent of the softened layer (5, 10 and 50 m, respectively) do not simulate slope failure. The lowering of the clay shale properties appeared to trigger tensile failure in the upper area of the slope and the propagation of the discontinuity SL3.1 when the layer was extended a length of 50 m under the slab. In the simulations represented in the lower row (Fig. 9) the extent of the layer was fixed at 50 m, and clay shale properties gradually changed. The elements located near the failure surface seem to yield when the initial clay shale properties were reduced by 85 %. The shape of the failure detachment

524 surface was correctly reproduced by the model, showing the backward propagation in the lower sector of the
525 scarp. Areas with higher tensile strain displaying a vertical shape were detected at the top of the slab, about 100
526 m to the rear of the cliff. Similar features were recognized in the field, both pre and post-failure, as shown in Fig.
527 10.
528 The reduced clay shale values were compared with those derived from field and laboratory tests conducted by
529 Gibertoni (2007) after the 2006 landslide for the softened layer (
530 Table **3**). The cohesion values are very similar, while the friction angle obtained from the simulations appears to
531 be very low in respect to the ones measured in the laboratory. In particular, the friction angle was derived from
532 consolidated drained shear tests on two specimens sampled in the San Leo northern area. It should be
533 emphasised that (i) the critical values of the clay layer properties derived are dependent upon failures occurring
534 within the rock mass and (ii) the laboratory test results may indicate higher bound laboratory values for friction
535 and not lower-bound field scale softened values.

536

537 **Table 3.** *Comparison between the parameters of the softened clayey layer derived from laboratory tests (Gibertoni,2007)*
538 *and from numerical simulations*

|	Cohesion (kPa)	Cohesion (residual) (kPa)	Friction angle (°)	Friction angle (residual) (°)
Lab tests	9-10	0-5	16-20	10-16
Simulations (80%)	8	6.4	5.6	3.9
Simulations (90%)	6	4.8	4.2	2.9

539
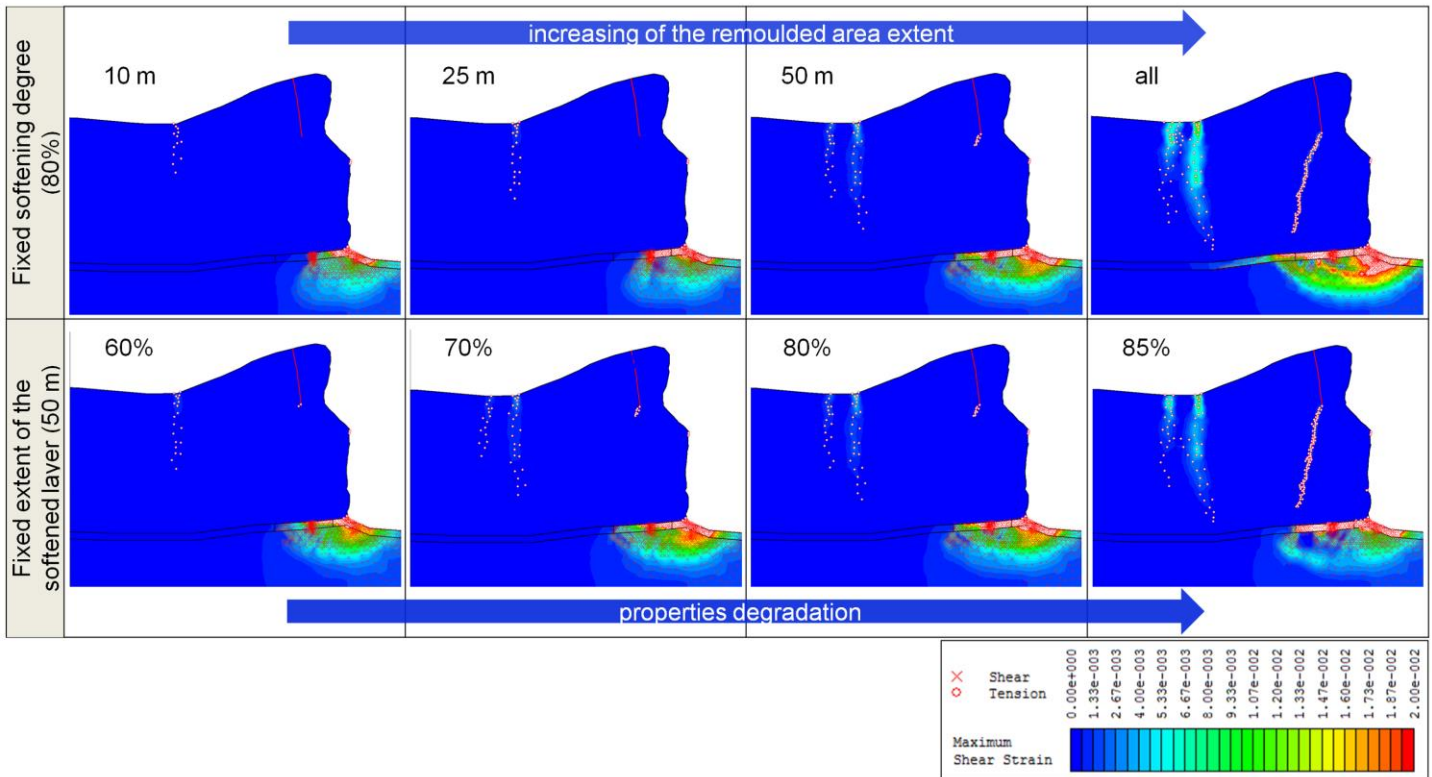
540

541 **Fig. 9.** *Results of the SCSL simulations. Upper row: Degree of softening fixed and increasing length of extent of the*
542 *softened layer (from left to right); lower row: fixed length of extent of softened layer and lowering of the mechanical*
543 *properties of the layer (from left to right)*

Fig. 10. *Views of the east cliff, before (a, b) and after (c) the 2014 failure. SL3.1 is shown as a red dotted line; discontinuities having an orientation similar to SL3.1 are highlighted as yellow dotted lines. b) Orthophoto of the NE cliff (Bing), the yellow dotted lines indicate discontinuities (detected also in the field) while the evidence interpreted as the discontinuity SL3.1 is indicated with a red dotted line.*

3.4   Undermining of the Slab (US)

In the US simulations the strain propagation also initiates from the lower part of the discontinuity SL3.1 and propagates down- and backwards (Fig. 11a). The SRF for each stage of the simulation are plotted against the meters of clay shale removed, e.g. the degree of undermining. The critical SRF = 1 is reached at between 22.5 and 25 m of excavation (Fig. 12). Tensile strain is recorded in the inner part of the slab, probably also including the effects of increase in joint aperture. As anticipated, displacements and yield in the clay shales are mostly recorded in the first stages of the simulation, i.e. reproducing the recent evolution of the slope and the related stress history (stage 1 to stage 5). However, additional shear yielding and movements can be correlated to the overburden load of the slab. In stage 6 the weight of the plateau is supported by a continuous clay layer, while in the following stages the progressive undermining, i.e. the removal of 2.5m wide clay shales slices as illustrated in Fig. 5b, results in a decrease of the clay shale area on which the weight of the plateau is distributed. This process can lead to a stress-induced softening of the clayey material. Moreover, the clayey material located below the removed slice can be subjected to swelling induced by unloading. In the present model, slices of 2.5 m are removed suddenly, while the natural erosion process would develop over a long time period, thus both displacements and stresses induced in the clay shales can be overestimated.

566
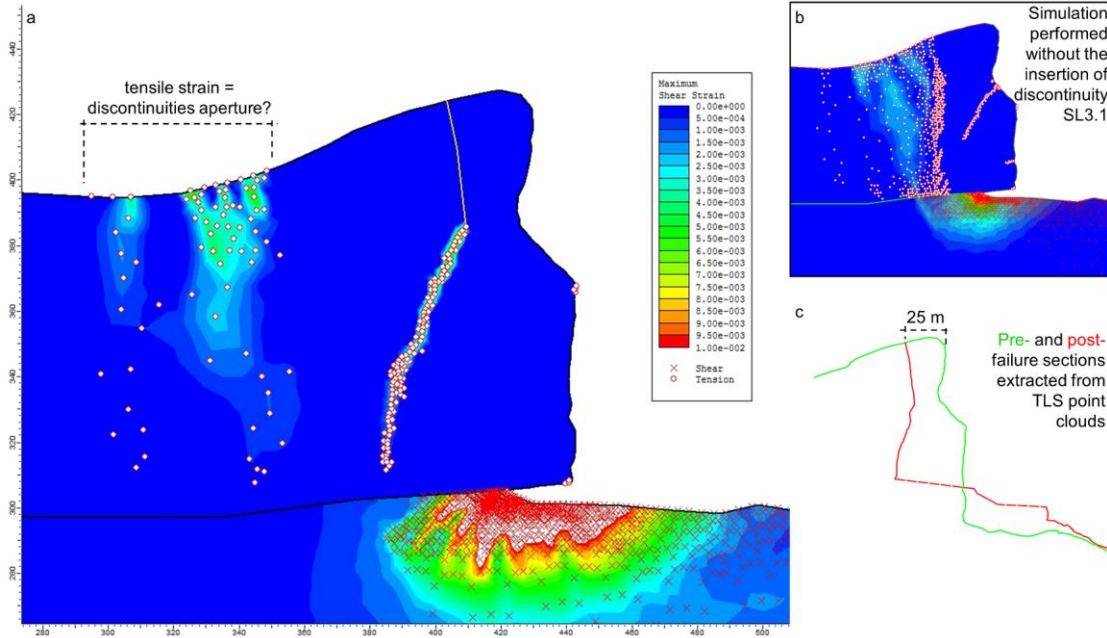
567 ***Fig. 11.*** *Results of the US simulations: a) Maximum shear strain measured at stage 14; b) US model results with no pre-*
568 *existing discontinuities; c)Pre- and post-landslide sections extracted from TLS point clouds*
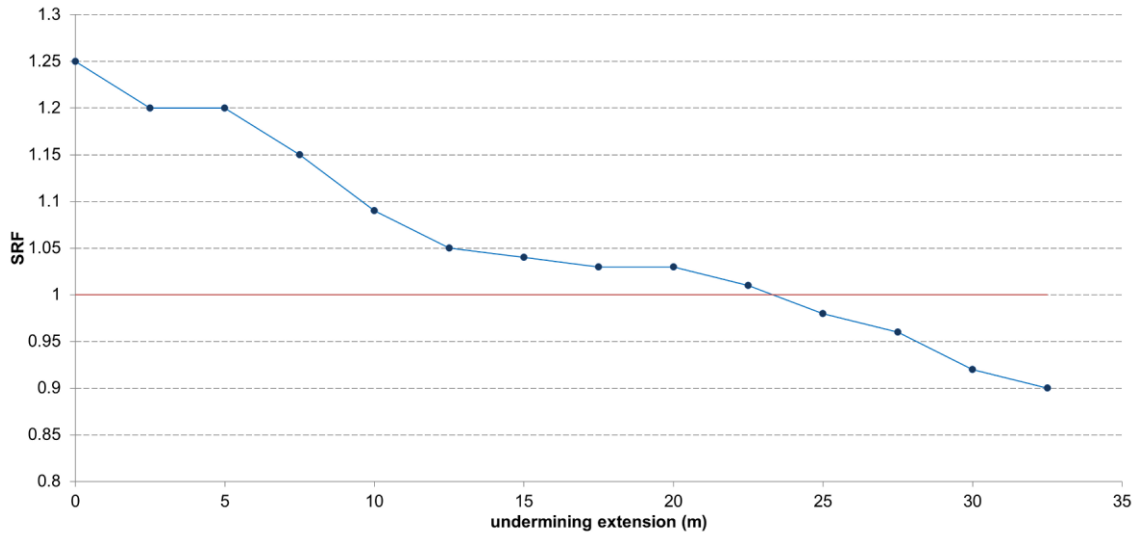
569
570 ***Fig. 12*** *SRF for each stage of the simulation, plotted against the length in meters of removed clay shales*
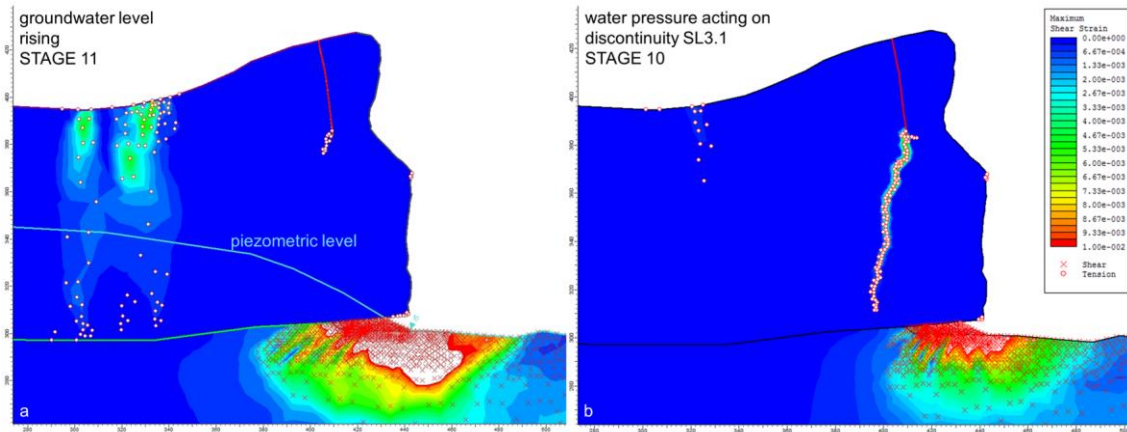
571 ### 3.3 Groundwater

572 The insertion of the elevated piezometric line in the US simulation (Fig. 13a) led to a general deterioration in the
573 stability conditions of the slope. In particular, in the model without the insertion of the piezometric line, the
574 failure developed at stage 15 (about 22.5 m of undermining) while, taking into account the piezometric line, the
575 failure developed at stage 12 (about 15 m of undermining). Thus, the groundwater level increase was simulated
576 at the 11th stage. As shown in Fig. 13a, the results of the simulation highlight that this process alone was not
577 sufficient to trigger the instability. The water pressure acting on the main detachment discontinuity (Fig. 13b)
578 can be considered a probable triggering factor. In fact, as illustrated in Fig. 13b, the inclusion of water pressure
579 led to the failure at stage 10 (about 10 m of undermining). It should be noted that modelling the rise in
580 groundwater level alone does not allow the role of water flow in terms of weathering and erosion to be assessed.
581 In fact, an increase in groundwater level might imply an effective increase of water seepage velocity and thus an

582 enhancement in erosional and softening processes acting on the clay shales layer. This phenomenon was not
583 simulated in the model.

584

585 **Fig.13.** *Results of the evaluation of the groundwater effects in the US simulation: a) effects of the rise in groundwater level*
586 *(about 4 m) at the 11^h stage of the simulation; b) effects of the water pressure acting on discontinuity SL3.1 at the 10th stage*
587 *of the simulation*

588   **3.4   FEM Voronoi-DFN model**

589 Results for a range of different models were obtained by varying the degree of persistence of the pre-existing
590 joints (25, 50 and 75% of the total length of the joint plane) and highlight the importance of discontinuity
591 persistence on the slope failure mechanism. In the case of a joint persistence equal to 25%, slope failure was not
592 simulated even with as much as 32.5 m of undermining, i.e. 10 m more than in the previous US simulations. In
593 contrast in the simulations performed with a joint persistence degree equal to 75% the slope failure was
594 simulated at between 10 and 15 m of undermining. Due to a higher fracture density, the jointed medium appears
595 to behave more like a continuum, showing a failure surface similar to that resulting from the analysis conducted
596 without any discontinuity (nor the SL3.1), shown in Fig. 11b; thus, the failure mechanism was not correctly
597 simulated. Finally, results of the simulation performed using a joint persistence of 50% are shown in Fig. 14. The
598 failure surface follows the main joint in the upper area of the cliff. In the lower portion both the joints belonging
599 to the simple DFN, e.g. the pre-existing joint sets and the Voronoi joint network are involved in the slope failure.
600 The results are representative of the actual failure surface. The different simulations performed for the last
601 scenario (joint persistence = 50%) suggested that, in addition to the joint persistence, the positions of the pre-
602 existing joints also plays a role in the definition of the critical degree of undermining for slope failure.

603
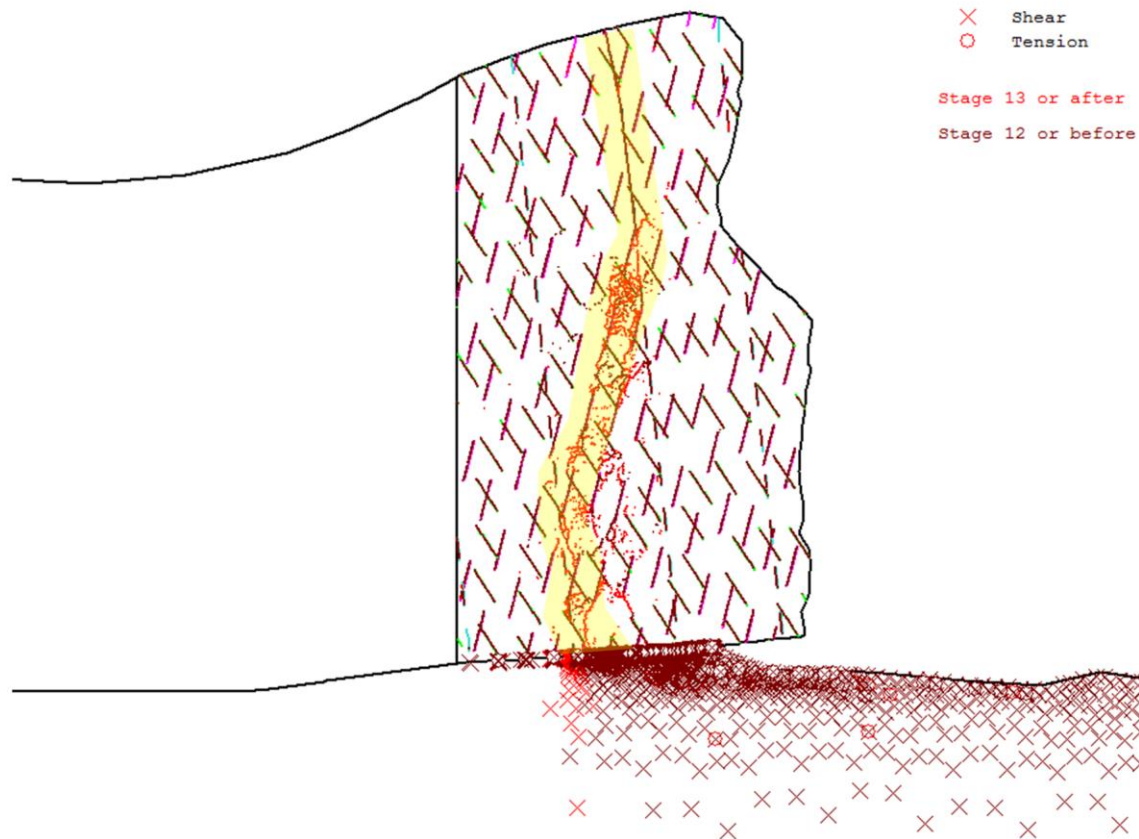
Fig.14. *Results of the Voronoi simulation, shown in red are the joints yielded at the failure stage and in dark red the joints yielded at previous stages of the simulation. Non-yielded joints are represented with their original colour (green, magenta and blue). Failures in the clay shale substratum are only partially shown, for visualization purposes.*

The Voronoi approach allowed highlighting of the fracture propagation through the intact rock mass and interaction with the pre-existing joints and also more realistic simulation of the detachment mechanisms. Some fracture of intact rock bridges can also be seen in areas not directly involved in the slope failure phenomena, probably related to boundary induced effects developing between the area with and without the Voronoi-network, or to the tensile stress developed in the inner part of the slab, visible also in the previous simulations.

Discussion

Our research has focused on the effects of the groundwater within the slab on the clay shale unit and consequently on the stability of the vertical and overhanging rock cliffs bordering the slab itself. The 2D FEM code Phase2 has allowed realistic simulation of the 2014 San Leo failure, reinforcing the evidence of secondary toppling phenomenon acting at the edges of the plateau.

The whole slope failure process can be summarized as follows. The aquifer hosted within the fractured slab, due to its relatively higher secondary permeability in comparison with the lower clay-rich units, favours the development of perennial and ephemeral springs at the contact between the two units. Chemical and physical processes, mainly associated with the interaction of clay shales with groundwater, promote softening of a basal layer which, associated with seepage erosion and groundwater sapping processes, led to the progressive removal of material at the toe of the slab. In the bedrock headwall, where favourable joint intersections are present, caves develop leading to the progressive undermining, collapse and retreat of the headwall itself. Moreover, creep and shallow landslides contribute to the removal of material. The cliff becomes progressively unstable and undergoes large-scale landslides due to falls or topples. The resulting landslide deposits may cause an undrained loading on clay-rich units (both on bedrock and on loose landslide and slope deposits), which in turn leads to the reactivation or to the acceleration of slow-moving earth slides or flows in gullies. In addition, the stress related to

628   the rock failure may contribute to the opening and increase in aperture of discontinuities within the rock slab,
629   enhancing and promoting future slope processes.
630   The model simulations include the effects of groundwater flow in the slab and at the contact with the underlying
631   clay shale layer by introducing (1) the lowering of the mechanical properties of a relatively thin clayey layer
632   underneath the cliff (illustrated by SCSL simulations) or (2) the removal of substratum slices to simulate the
633   undermining of the slab (US simulations). Both these mechanisms have been observed in the field. In these
634   preliminary simplified models they were treated separately but in practice they probably act together. In fact, the
635   two effects are actually parts of the same process: while the shallower layer of clay shale is progressively eroded
636   the remaining portion is subjected to strength degradation and vice-versa. As suggested by Yoshida et al. (1991)
637   the softening can, in fact, be considered more severe near the ground surface than at depth, because at shallow
638   depths both internal (due to water absorption upon unloading) and external (due to weathering effects) softening
639   takes place. The removal of clays can be seen as the last stage of the softening phenomenon. The role of the clay
640   shale substratum is fundamental in the initiation of the failures affecting the rock slab. Evans (1981) excluded
641   the possibility of a relevant instability triggered by the material removal at the toe of the cliff, admitting that only
642   minor failures (vertical column ranging from 0.5 to 1 m wide) are possible. The important difference between his
643   work and our research is the extension of the undercutting. In fact, areas investigated by Evans (1981) were
644   characterized by a maximum erosion depth in the order of 2 m. In the same work, Evans recognized that the size
645   of the rock mass involved in the failure is determined by the extent of basal weathering and undercutting. In the
646   San Leo case study, the undermining necessary to initiate massive instability in the cliff is similar to that
647   observed in the field (about 20 m).
648   The comparison between the critical mechanical properties of the clay shales as derived from the numerical
649   analyses and those determined from laboratory testing shows similar values for cohesion, whereas the friction
650   angle obtained from the model simulations appears to be lower. This comparison can be only considered as
651   purely indicative, since it is influenced by several factors, i.e. scale and sampling effects, the presence of micro-
652   and meso-structures and weakness planes in the clay shales and the influence of the rock mass properties on the
653   derived critical clay shales properties.
654   At the same time, it must be pointed out that Di Maio and Fenelli (1994), Picarelli et al. (2000) and Di Maio et
655   al. (2004) found similar differences (about 70%) by analysing the residual shear strength of smectite-rich clay
656   shales in distilled water and in NaCl solution. In particular they found a residual friction angle equal to 4°-6° for
657   the specimen tested in distilled water and about 15° for the one tested in the saturated salt solution.
658   Moreover Botts (1986), analysing the softening behaviour of Pierre shale, found a 75 % decrease in strength
659   after one drying and rewetting cycle (reduction of 6° in the internal degree of friction, loss in cohesion from 848
660   to 0 kPa).
661   With reference to the San Leo case, the lowering of the cohesion and friction angle in clay shales can be further
662   explained by a combination of the two processes, i.e. the softening associated with change in pore water
663   chemistry and a decrease in soil suction.
664   Finally, as introduced by Terzaghi (1936) and Skempton (1970), slope unloading might play an important role in
665   the softening of fissured over-consolidated clays, which, as a consequence, can experience some reduction in
666   shear strength. Furthermore, the changes in the slope morphology, i.e. the cliff undercutting, can lead to stress
667   concentrations in the underlying clayey layer and thus in the development of damage and yielding.
668   Regarding the values chosen for the rock mass properties, the tensile strength seems to influence the onset of
669   failure. A similar importance of this parameter was noticed also by Styles et al. (2011) studying the detrimental
670   effect of a wave-cut notch at Chalk cliffs in southern England.
671   Another important factor is the presence of almost-vertical discontinuities at the top of the cliff. Without
672   considering the vertical discontinuities, the actual failure mechanism cannot be reproduced. As shown by the
673   simulations, the increase in the aperture of these discontinuities is favored by the tensile stress developing in the
674   upper part of the slab prior to the failure. In fact, the shape and the position of the tensile strain areas in the
675   models agree closely with the fractures mapped in the field before and after the failure. It appears that the
676   historic failure induced slope displacements provide the conditions for successive instability events. Tensile
677   failure and subsequent growth of tension cracks at the top of the slope were also reported by Styles et al. (2011)
678   due to chalk cliff undercutting. In this case, probably due to the different mechanical properties of the
679   investigated weak chalk rock masses and to the absence of a well-developed discontinuity at the top of the cliff,

680 the obtained failure mechanism was slightly different with stress concentration fracture developing from the
681 notch and subsequent migrating upward. The failure surface reported in Styles et al. (2011) also shows a
682 different geometry, without the backward propagation typical of the San Leo 2014 landslide. In the simulation
683 performed without the insertion of the upper discontinuity, the failure surface geometry appears to be more
684 similar to that described by Styles et. al. (2011).
685 The Voronoi approach was used to represent fracture propagation within the intact rock mass, transforming a
686 continuum medium into a combination of independent blocks. In this way, it was possible to include some of the
687 benefits of the discontinuum methods in a continuum code. The Phase2 Voronoi-DFN model successfully
688 simulates the complex failure mechanisms, including both the opening of pre-existing fractures and intact rock
689 bridge fracturing. In the present work the Voronoi approach was used to confirm and integrate the results
690 reached in the previous simulations. Gao and Stead (2014) and Havaej et al. (2014) suggested that, for the
691 Voronoi tessellation implemented in UDEC, a calibration of the block contact properties is required. The
692 properties used in the simulations for the FEM Voronoi joint network seem to reproduce correctly the failure
693 mechanism, so in this preliminary analysis no attempt was made in the calibration of the micro-properties.
694 The results agree closely with the back analysis carried out on the same slope using the DEM 3DEC (Spreafico
695 et al. 2015c). Moreover, in the present simulations, the continuum Phase2 numerical code allows the backward
696 propagation of the detachment surface to be reproduced.
697 In field observations on the 2014 San Leo landslide scar and deposit, rock bridges can be clearly identified.
698 Given their importance in controlling the failure, as showed in the Voronoi simulations, the quantification of
699 their amount could lead to an enhanced understanding of the mechanisms leading to the slope failure. Increasing
700 attention has recently been given to the study of rock bridges however the quantification of rock bridge content
701 remains an important area for future research and is not trivial. Tuckey (2012) attempted to develop a procedure
702 for the estimation of rock bridge content using remote sensing techniques and highlighted the geotechnical
703 challenges. In our simulations only the breaking of in-plane rock bridges (sensu Tuckey, 2012) could be
704 analyzed, due to the 2D software. Analysis regarding the rupture of out-of-plane rock bridges and the
705 interlocking between rock blocks would provide further insight on the acting failure mechanisms.
706 In the last two major San Leo slope failures, i.e. the 2006 and the 2014 events, an undermined area at the base of
707 the cliff was recognized prior to the failure. Furthermore, oxidation was recognized on the joint set with an
708 orientation parallel to the cliff face, indicating water circulation and thus their pre-existence. The difference in
709 the detached rock volumes can probably be explained by a combination of the degree of undermining and the
710 position of the pre-existing discontinuities sub-parallel to the cliff orientation. In the case of sub-vertical
711 discontinuities closer to the rock cliff, a lesser degree of undermining would be sufficient to trigger the
712 instability.
713 Some limitation of the present work can be recognized in an inability to fully model the evolution of the failure
714 with time. In fact, although the different excavation stages can roughly simulate the relative time, the implicit
715 solver implemented in the code Phase2 allows only one solution for each stage. An explicit modelling method,
716 e.g. with a brittle fracture finite-discrete element code such as Elfen (Rockfield 2001), should be used to more
717 fully investigate this aspect.
718 Additional work should be undertaken on the simulation of the clay shales behavior, reproducing more closely
719 the erosion processes and the stresses acting on the surficial layer of this unit. The monitoring of the
720 displacements in this unit and the use of more suitable constitutive criteria, to describe the effects of time and
721 strain-dependent softening effects on overconsolidated clays (Yoshida et al., 1990; Stead, 2016), may help to
722 better constrain the slope failure.
723 Further development should concentrate on the definition of the groundwater flow path within the slab and on
724 the estimation of the seepage erosion rate induced within the underlying clayey units. It would be of great
725 interest to evaluate the time necessary to produce an undermining similar to that analyzed in the present work, in
726 order to estimate the return period of comparable failures. The work proposed by Miscevic and Vlastelica (2014)
727 can be cited as an example of such an estimation; they quantified a weathering rate for marls underlying a
728 sandstone layer near Split (Croatia) as 10 cm/year, monitoring the length of the overhanging sandstone layer
729 through the time (8 years).
730 The detection of the areas characterized by a higher spring discharge rate and thus by a more accelerated seepage
731 erosion would also help in the identification of the zones more susceptible to instability and ensure the design of

732 effective countermeasure works.

733 **Conclusion**

734 Back analyses through numerical models can provide further insights and understanding of mechanisms of rock
735 slope failure. The present study provides an in depth understanding of the factors influencing the long-term
736 evolution of lateral spreads where brittle rock masses overlie a soft substratum. In particular, the onset of
737 secondary toppling mechanisms, developing at the edges of fractured plateaux was reinforced through the back
738 analysis of the 2014 San Leo landslide. These processes can affect similar slabs subjected to lateral spread
739 phenomena. The role of several factors, both external and internal to the slope system, have been investigated
740 with respect to similar slope instabilities, i.e. marked contrast between the mechanical properties of the overlying
741 and underlying geological units and the resulting stress distributions within the slabs, stress relief in the stiffer
742 overlying units due to the erosion of the underlying softer units, and overburden load due to the rock slabs
743 causing deformation of the underlying weaker terrains. Here, we prove that groundwater plays an important role
744 in the evolution of the whole slab, enhancing weathering and subsequent geomorphological processes at the base
745 of the cliffs. The importance of the processes developing in the clay shale unit were highlighted.
746 The paper presents an innovative application of FEM-DFN-Voronoi to rock slope stability analysis which has
747 not been applied to the authors' knowledge within the previous literature to the back-analysis of a major
748 landslide. Thanks to the coupling between Finite Element Voronoi approach and a simple DFN, the simulation
749 of fracture propagation along pre-existing discontinuities and the breaking of intact rock bridges was simulated.

754

755 **References**

756 Agliardi, F., Crosta, G. and Zanchi, A., 2001. Structural constraints on deep-seated slope deformation kinematics.
757 Engineering Geology, 59, pp.83–102. DOI: 10.1016/S0013-7952(00)00066-1

758 Al-Badran, Y., 2011. Volumetric yielding behavior of unsaturated fine-grained soils. Ruhr-Universität Bochum. PhD
759 thesis.

760 Alzo'ubi, A.M., 2009. The effect of tensile strength on the stability of rock slopes. University of Alberta. PhD thesis.

761 Badioli, L., 2012. Analisi strutturale della rocca di San Leo. BSc thesis, University of Bologna (unpublished).

762 Barton, N., and Choubey, V., 1977. The shear strength of rock joints in theory and practice. Rock Mech., 10, pp.1-54

763 Benedetti, G., Bernardi, M., Bonaga, G., Borgatti, L., Continelli, F., Ghirotti, M., Guerra, C., Landuzzi, A., Lucente, C.C.
764 and Marchi, G., 2013. San Leo: Centuries of coexistence with landslides C. Margottini, P. Canuti, and K. Sassa,
765 eds. Landslide Science and Practice, 6(IV), pp.529–537. DOI: 10.1007/978-3-642-31319-6

766 Benko, B., 1997. Numerical modelling of complex slope deformations. University of Saskatchewan. PhD thesis.

767 Bittelli, M., Valentino, R., Salvatorelli, F. and Rossi Pisa, P., 2012. Monitoring soil-water and displacement conditions
768 leading to landslide occurrence in partially saturated clays. Geomorphology, 173-174, pp.161–173. DOI:
769 10.1016/j.geomorph.2012.06.006

770 Bonnard, C., Forlati, F., and Scavia, C., 2004. Identification and mitigation of large landslide risks in Europe: Advances
771 in risk assessment. CRC Press.

772 Borgatti, L., Guerra, C., Nesci, O., Romeo, R.W., Veneri, F., Landuzzi, A., Benedetti, G., Marchi, G. and Lucente, C.C.,
773 2015. The 27 February 2014 San Leo landslide (northern Italy). Landslides, (July 2014), pp.387–394. DOI:
774 10.1007/s10346-015-0559-4

775   Botts, M.E., 1986. The effect of slaking on the engineering behavior of clay shales. University of Colorado. PhD Thesis

776   Bozzano, F., Bretschneider, A. and Martino, S., 2008. Stress-strain history from the geological evolution of the Orvieto
777   and Radicofani cliff slopes (Italy). Landslides, 5(March), pp.351–366. DOI: 10.1007/s10346-008-0127-2

778   Calabresi, G. and Scarpelli, G., 1985. Effects of swelling caused by unloading in overconsolidated clays. In XI ICSMFE
779   Conference. San Francisco: AA Balkema, pp. 411–414.

780   Casagli, N., 1994. Fenomeni di insatbilità in ammassi rocciosi sovrastanti un substrato deformabile: analisi di alcuni
781   esempi nell'Appennino Settentrionale. Geologica Romana, 30, pp.607–618.

782   Cencetti, C., Conversini, P. and Tacconi, P., 2005. The Rock of Orvieto (Umbria , Central Italy). Giornale Di Geologia,
783   1, pp.103–112. DOI: 10.1474/GGA.2005-01.0-10.0010

784   Christianson, M.C., Board, M.P. and Rigby, D.B., 2006. UDEC simulation of triaxial testing of lithophysal tuff. In In
785   Proceedings of Golden Rocks 2006, The 41st U.S. Symposium on Rock Mechanics (USRMS): "50 Years of
786   Rock Mechanics - Landmarks and Future Challenges". American Rock Mechanics Association.

787   Cruden, D.M. and Varnes, D.J., 1996. Landslides investigation and mitigation. In A. K. Turner and R. L. Schuster, eds.
788   Landslide types and process. National Academy Press, pp. 36–75.

789   D'Ambra, S., Giglio, G. and Lembo-Fazio, A., 2004. Arrangement and stabilization of the San Leo cliff. In International
790   Symposium Interpraevent 2004 – Riva/Trient. pp. 103–114.

791   Delmonaco, G., Margottini, C. and Spizzichino, D., 2009. Low impact interventions for the preservation of Cultural
792   Heritage: the dying town of Civita di Bagnoregio (Central Italy) and the killer landslide. In Protection of
793   Historical Buildings, PROHITECH 09. London: Taylor and Francis Group, pp. 1455–1459.

794   Diederichs, M.S., Lato, M., Hammah, R. and Quinn, P., 2007. Shear strength reduction approach for slope stability
795   analyses. In Proceedings of the 1st Canada-US Rock Mechanics Symposium. pp. 319–327.

796   Diersch, H.J.G., 2005. FEFLOW finite element subsurface flow and transport simulation system. Reference manual.

797   Di Giusto, M., 2009. Ispezione delle condizioni di stabilità del muro di contenimento del piazzale superiore del forte di
798   San Leo (PU).

799   Di Maio, C., 1996a. Exposure of bentonite to salt solution: osmotic and mechanical effects. Geotechnique 46(4), pp. 695-
800   707. DOI: 10.1680/geot.1996.46.4.695

801   Di Maio, C., 1996b. The influence of pore fluid composition on the shear strength of some natural clayey soils. In
802   Proceedings of the international Symposium on Landslides, 2, pp. 1189-1194.

803   Di Maio, and C. Fenelli, G.B., 1994. Residual strength of kaolin and bentonite: the influence of their constitutive pore
804   fluid. Geotechnique 44(4), pp. 217–226. DOI: 10.1680/geot.1994.44.2.217

805   Di Maio, C., Santoli, L. and Schiavone, P., 2004. Volume change behaviour of clays: The influence of mineral
806   composition, pore fluid composition and stress state. Mechanics of Materials, 36, pp. 435-451.

807   Di Maio, C., Scaringi, G. and Vassallo, R., 2014. Residual strength and creep behaviour on the slip surface of specimens
808   of a landslide in marine origin clay shales: influence of pore fluid composition. Landslides, 12, pp. 657-667.
809   DOI: 10.1007/s10346-014-0511-z.

810   Di Maio, C., Vassallo, R. and Vallario, M., 2013. Plastic and viscous shear displacements of a deep and very slow
811   landslide in stiff clay formation. Engineering Geology, 162, pp.53–66. DOI: 10.1016/j.enggeo.2013.05.003

812   Dramis, F., 1985. Slope geomorphology. In Italian Research on Physical Geography and Geomorphology: an overview.
813   Bologna: C.N.R.-Technoprint, pp. 5–11.

814   Dunne, T. 1980. Formation and controls of channel networks. Prog. Phys. Geogr., 4, pp. 211 –239.

815   Enser srl, 2014. Lavori di somma urgenza per il monitoraggio ed,approfondimento conoscitivo della nuova morfologia dei
816   luoghi del versante nord della rupe di San Leo (RN) interessata da crollo,

817   Evans, R.S., 1981. An analysis of secondary toppling rock failures—the stress redistribution method. Quarterly Journal of

818   Engineering Geology and Hydrogeology, 14(2), pp.77–86.

819   Fanti, R., Gigli, G., Lombardi, L., Tapete, D. and Canuti, P., 2012. Terrestrial laser scanning for rockfall stability analysis
820   in the cultural heritage site of Pitigliano (Italy). Landslides, 10, pp.409–420. DOI: 10.1007/s10346-012-0329-5

821   Fredlund, D.G. and Rahardjo, H., 1993. Soil mechanics for unsaturated soils. John Wiley and Sons.

822   Fredlund, D.G. and Morgenstern, N.R., 1978. The shear strength of unsaturated soils. Canadian Geotechnical Journal,
823   15(3), pp.313 – 321.

824   Freeze, R.A. and Cherry, J.A., 1979. Groundwater, Prentice-Hall, Englewood Cliffs, NJ.

825   Froldi, P., Mantovani, S., Lunardi, P. and Podesta, G., 1994. Argille Scagliose complex in northern Italy: the geotechnical
826   characterisation. In Proceedings, International Association of Engineering Geology, 7th International Congress:
827   Lisbon. pp. 459–468.

828   Gao, F.Q. and Stead, D., 2014. The application of a modified Voronoi logic to brittle fracture modelling at the laboratory
829   and field scale. International Journal of Rock Mechanics and Mining Sciences, 68, pp.1–14. DOI:
830   10.1016/j.ijrmms.2014.02.003

831   Giardino, M., Mortara, G., Borgatti, L., Nesci, O., Guerra, C., Lucente, C.C., 2015. Dynamic geomorphology and
832   historical iconography. Contributions to the knowledge of environmental changes and slope instabilities in the
833   Apennines and the alps. In: Lollino, G., Giordan, D., Marunteanu, C., Christaras, B., Yoshinori, I., Margottini, C.
834   (Eds.), I, Engineering Geology for Society and Territory Vol. Volume 8. Springer International Publishing, pp.
835   463-468.Gibertoni, F., 2007. Analisi di una frana in località San Leo (PU). MSc. Thesis, Università di Bologna.

836   Gigli, G., Frodella, W., Mugnai, F., Tapete, D., Cigna, F., Fanti, R., Intrieri, E. and Lombardi, L., 2012. Instability
837   mechanisms affecting cultural heritage sites in the Maltese Archipelago. Natural Hazards and Earth System
838   Science, 12, pp.1883–1903. DOI: 10.5194/nhess-12-1883-2012

839   Goodman, R.E. and Bray, J.W., 1976. Toppling of rock slopes. In Rock Engineering for Foundations and Slopes. ASCE,
840   pp. 201–234.

841   Hammah, R.E., Yacoub, T.E., Corkum, B.C. and Curran, J.H., 2005. The shear strength reduction method for the
842   generalized Hoek-Brown criterion. In Proceedings of the American Rock Mechanics Association.

843   Hammah, R.E., Yacoub, T.E., Corkum, B., Wibowo, F. and Curran, J.H., 2007. Analysis of blocky rock slopes with finite
844   element shear strength reduction analysis. In Proceedings of the 1st Canada-US Rock Mechanics Symposium.
845   pp. 329–334.

846   Havaej, M., Stead, D., Eberhardt, E. and Fisher, B.R., 2014. Characterization of bi-planar and ploughing failure
847   mechanisms in footwall slopes using numerical modelling. Engineering Geology, 178, pp.109–120. DOI:
848   10.1016/j.enggeo.2014.06.003

849   Hoek, E., 1994. Strength of rock and rock masses. ISRM News Journal, 2(2), pp.4–16.

850   Hoek, E. and Brown, E.T., 1997. Practical estimates of rock mass strength. International Journal of Rock Mechanics and
851   Mining Sciences, 34(8), pp.1165–1186.

852   Hungr, O., Leroueil, S. and Picarelli, L., 2014. The Varnes classification of landslide types, an update. Landslides, 11,
853   pp.167–194.

854   ItascaTM, 2014a. 3DEC. Available at: http://www.itascacg.com.

855   ItascaTM, 2014b. UDEC. Available at: http://www.itascacg.com.

856   Kaşmer, Ö., Ulusay, R. and Geniş, M., 2013. Assessments on the stability of natural slopes prone to toe erosion, and man-
857   made historical semi-underground openings carved in soft tuffs at Zelve Open-Air Museum (Cappadocia,
858   Turkey). Engineering Geology, 158, pp.135–158. DOI: 10.1016/j.enggeo.2013.03.010

859   Kenney, T.C., 1967. The influence of mineralogic composition on the residual strength of natural soils. In Proceedings of
860   the Oslo Conference on Shear Strength Properties of Natural Soils and Rocks. pp.123-129.

861 Lamb, M. P., Howard, A. D., Johnson, J., Whipple, K. X., Dietrich, W. E. and Perron, J. T., 2006. Can springs cut
862   canyons into rock? J. Geophys. Res., 111, E07002. DOI:10.1029/2005JE002663.

863 Lu, N. and Godt, J., 2008. Infinite slope stability under steady unsaturated seepage conditions. Water Resources Research,
864   44 (November), pp.1–13. DOI 10.1029/2008WR006976

865 Mantovani, M., Devoto, S., Forte, E., Mocnik, A., Pasuto, A., Piacentini, D. and Soldati, M., 2013. A multidisciplinary
866   approach for rock spreading and block sliding Investigation In the north-western coast of Malta. Landslides,
867   10(5), 611-622.

868 Mesri, G. and Olson, R.E., 1970. Shear strength of montmorillonite. Geotechnique 20(3), pp. 261-270.

869 Miscevic, P. and Vlastelica, G., 2014. Impact of weathering on slope stability in soft rock mass. Journal of Rock
870   Mechanics and Geotechnical Engineering, 6, pp.240-250. DOI: 10.1016/j.jrmge.2014.03.006

871 Nakano, R., 1979. Geotechnical properties of mudstone of neogene tertiary in Japan. In Proc. Int. Symp. Soil Mechs., 1,
872   pp. 75-92.

873 Nash, D. J., 1996. Groundwater sapping and valley development in the Hackness hills, north Yorkshire, England. Earth
874   Surf. Processes Landforms, 21(9), pp. 781– 795.

875 Pasuto, A. and Soldati, M., 2013. Lateral spreading. In Treatise on Geomorphology. Elsevier, pp. 239–248. DOI:
876   10.1016/B978-0-12-374739-6.00173-1

877 Picarelli, L., 2015. Landslides in hard soils and weak rocks. Landslides, 12(4), p. 641. DOI: 10.1007/s10346-015-0591-4

878 Picarelli, L. and Di Maio, C., 2010. Deterioration processes of hard clays and clay shales. Engineering Geology Special
879   Publications: Weathering as predisposing factor to slope movements, 23, pp.15–32.

880 Picarelli, L., Di Maio, C., Olivares, L. and Urciuoli, G., 2000. Properties and behaviour of tectonized clay shales in Italy.
881   In Evangelista and Picarelli, eds. The geotechnics of hard soils-soft rocks. Rotterdam: Balkema, pp. 1211–1242.

882 Picarelli, L., Urciuoli, G., Mandolini, a. and Ramondini, M., 2006. Softening and instability of natural slopes in highly
883   fissured plastic clay shales. Natural Hazards and Earth System Sciences, 6(1985), pp.529–539. DOI:
884   10.5194/nhess-6-529-2006

885 Picarelli, L., Urciuoli, Ramondini, M. and Comegna L., 2005. Main features of mudslides in tectonised highly fissured
886   clay shales. Landslides, 2, pp.15–30. DOI: 10.1007/s10346-004-0040-2

887 Rampello, S., 1992. Some remarks on the mechanical behaviour of stiff clays: the example of Todi clay. In Experimental
888   Characterization and Modelling of Soils and Soft Rocks : A Workshop in Napoli. Napoli: Università degli Studi
889   di Napoli, pp. 131–190.

890 Ribacchi, R. and Tommasi, P., 1988. Preservation and protection of the historical town of San Leo (Italy). In Marinos and
891   Kuokis, eds. IAEG Int. Symp. on Engineering Geology of Ancient Works Monuments and Historical Sites.
892   Athens: Balkema, pp. 55–64.

893 Rockfield, 2001. ELFEN 2D/3D Numerical Modelling Package. Available at: http://www.rockfield.co.uk/.

894 Rocscience Inc., 2014a. Phase2. Available at: http://www.rocscience.com.

895 Rocscience Inc., 2014b. RocLab. Available at: http://www.rocscience.com.

896 Seedsman, R., 1986. The behaviour of clay shales in water. Can. Geotech. J., 23, pp 18-22.

897 Skempton, A. W., 1970. First-time slides in over-consolidated clays. Geotechnique, 20(3), pp. 320-324.

898 Soldati M., 2013. Deep-Seated Gravitational Slope Deformation. In: P.T. Bobrowsky (ed.), Encyclopedia of Natural
899   Hazards. Springer Netherlands, 151-155.

900 Spreafico, M.C., Cervi, F. and Borgatti, L., 2015a. Modelling groundwater and slope processes in a calcarenitic slab : the
901   case of San Leo (northern Apennines). Rendiconti Online della Società Geologica Italiana, 34, pp.23–27. DOI:
902   10.33.01/ROL.2015.31

903 Spreafico, M.C., Cervi, F., Marc, V., Borgatti, L., 2015b. Hydrogeological features of a highly fractured rock-slab.
904   Rendiconti Online della Società Geologica Italiana, 35, pp.283–287. DOI: 10.3301/ROL.2015.121

905 Spreafico, M.C., Francioni, M., Cervi, F., Stead, D., Bitelli, G., Ghirotti, M., Girelli, V.A., Lucente, C.C., Tini, M.A. and
906   Borgatti, L., 2015c. Back analysis of the 2014 San Leo landslide using combined terrestrial laser scanning and
907   3D distinct element modelling. Rock Mechanics and Rock Engineering. Available at:
908   http://link.springer.com/10.1007/s00603-015-0763-5.

909 Spreafico, M.C., Perotti, L., Cervi, F., Bacenetti, M., Bitelli, G., Girelli, V.A., Mandanici, E., Tini, M.A. and Borgatti, L.,
910   2015d. Terrestrial remote sensing techniques to complement conventional geomechanical surveys for the
911   assessment of landslide hazard: the San Leo case study (Italy). European Journal of Remote Sensing, 48, pp. 639-
912   660. DOI: 10.5721/EuJRS20154835#sthash.EWb2h2sA.dpuf

913 Stead, D., 2016. The influence of shales on slope instability. Rock Mechanics and Rock Engineering, 49:635–651

914 Sturzenegger, M. Sturzenegger, M. and Stead, D., 2012. The Palliser Rockslide, Canadian Rocky Mountains:
915   Characterization and modeling of a stepped failure surface. Geomorphology, 138(1), pp.145–161. DOI:
916   10.1016/j.geomorph.2011.09.001

917 Styles, T.D., Coggan, J.S. and Pine, R.J., 2011. Back analysis of the Joss Bay Chalk Cliff Failure using numerical
918   modelling. Engineering Geology, 120(1-4), pp.81–90. DOI: 10.1016/j.enggeo.2011.04.004

919 Terzaghi, K., 1936. Stability of slopes in natural clay. In Proceedings of the International Conference on Soil Mechanics
920   and Foundations, 1, pp. 161-165.

921 Tommasi, P., 1996. Stabilità di versanti naturali ed artificiali soggetti a fenomeni di ribaltamento. Rivista Italiana di
922   Geotecnica, 4.

923 Thornthwaite, C.W. and Mather, J.R., 1957. Instructions and tables for computing potential evapotranspiration and the
924   water balance. Publ. Climatol., 10, 3.

925 Tuckey, Z., 2012. An integrated field mapping-numerical modelling approach to characterising discontinuity persistence
926   and intact rock bridges in large open pit slopes, MSc. Thesis, Simon Fraser University.

927 Vannucchi, P., Maltman, A., Clennel, M. and Bettelli, G., 2003. On the nature of scaly fabric and scaly clay. Journal of
928   Structural Geology, 25(5), pp.673–688. DOI: 10.1016/S0191-8141(02)00066-4

929 Vivas Becerra, J., 2014. Groundwater characterization and modelling in natural and open pit rock slopes. MSc. Thesis,
930   Simon Fraser University.

931 Vlcko, J., 2004. Extremely slow slope movements influencing the stability of Spis Castle, UNESCO site. Landslides, 1,
932   pp.67–71. DOI: 10.1007/s10346-003-0007-8.

933 Yoshida, N., Morgenstern, N. R., and Chan., D. H., 1990. A failure criterion for stiff soils and rocks exhibiting
934   softening. Canadian Geotechnical Journal, 27(2), pp. 195-202. DOI: 10.1139/t90-023

935 Yoshida, N., Morgenstern, N. R., and Chan, D. H., 1991. Finite-element analysis of softening effects in fissured, over
936   consolidated clays and mudstones. Canadian Geotechnical Journal, 28(1), pp. 51-61. DOI: 10.1139/t91-006